NASA CONTRACTOR REPORT

NASA CR-1932

NASA CR-1932

SUBSONIC AND SUPERSONIC STATIC AERODYNAMIC CHARACTERISTICS OF A FAMILY OF BULBOUS BASE CONES MEASURED WITH A MAGNETIC SUSPENSION AND BALANCE SYSTEM

by M. Vlajinac, T. Stephens, G. Gilliam, and N. Pertsas

Prepared by
MASSACHUSETTS INSTITUTE OF TECHNOLOGY
Cambridge, Mass. 02139
for Langley Research Center

NATIONAL AERONAUTICS AND SPACE ADMINISTRATION • WASHINGTON, D. C. • JANUARY 1972

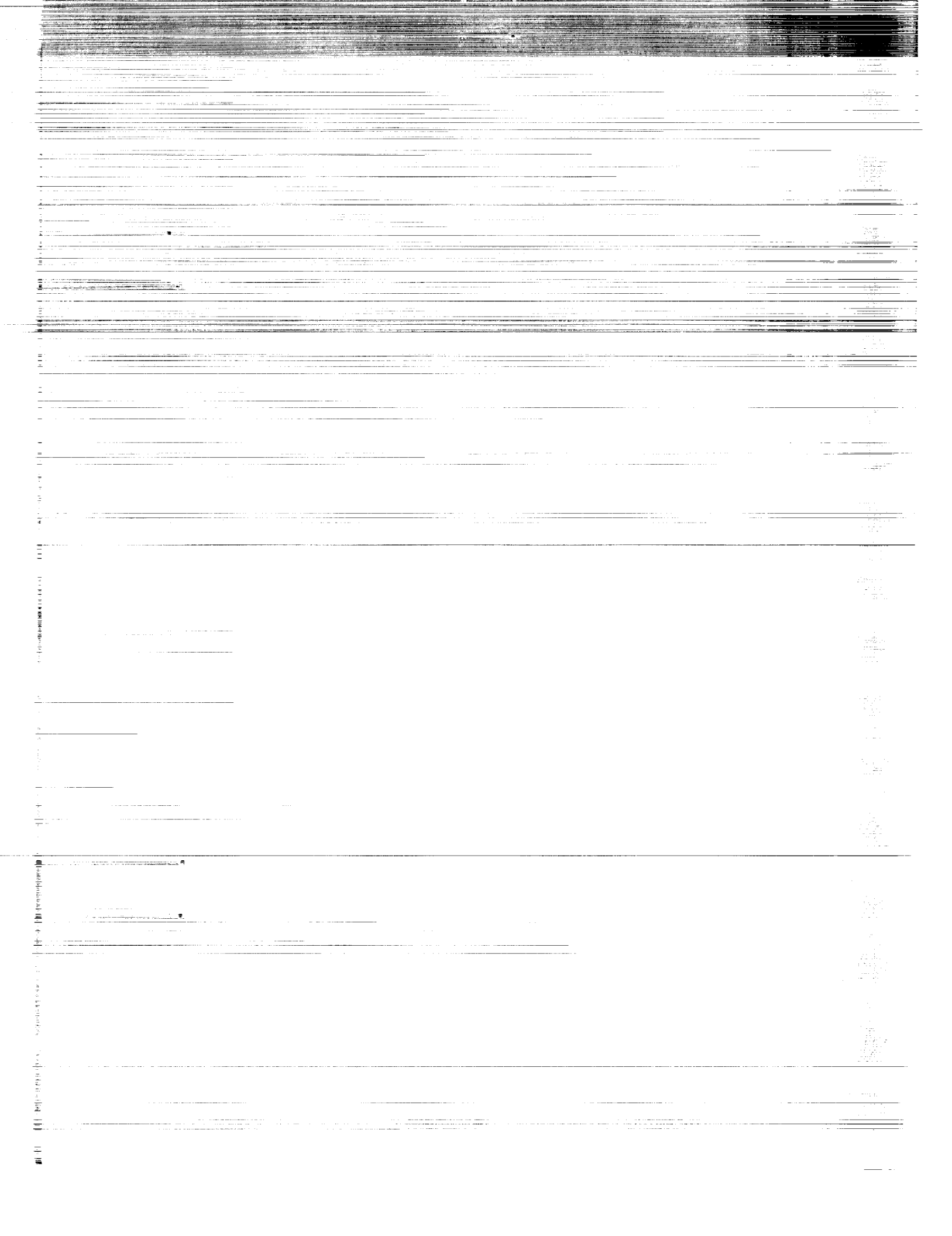

1. Report No.	2. Government Accession No.	3. Recipient's Catalog No.
NASA CR-1932		

4. Title and Subtitle	5. Report Date
SUBSONIC AND SUPERSONIC STATIC AERODYNAMIC CHARACTERISTICS OF A FAMILY OF BULBOUS BASE CONES MEASURED WITH A MAGNETIC SUSPENSION AND BALANCE SYSTEM	January 1972
	6. Performing Organization Code

7. Author(s)	8. Performing Organization Report No.
M. Vlajinac, T. Stephens, G. Gilliam, and N. Pertsas	Technical Report 166
	10. Work Unit No.

9. Performing Organization Name and Address	11. Contract or Grant No.
Massachusetts Institute of Technology Aerophysics Laboratory Cambridge, Massachusetts 02139	NAS1-8658
	13. Type of Report and Period Covered Contractor Report

12. Sponsoring Agency Name and Address	14. Sponsoring Agency Code
National Aeronautics and Space Administration Washington, D. C. 20546	

15. Supplementary Notes

16. Abstract

Results of subsonic and supersonic wind-tunnel tests with a magnetic balance and suspension system on a family of bulbous based cone configurations are presented. At subsonic speeds the base flow and separation characteristics of these configurations is shown to have a pronounced effect on the static data. Results obtained with the presence of a dummy sting are compared with support interference free data. Support interference is shown to have a substantial effect on the measured aerodynamic coefficient.

17. Key Words (Suggested by Author(s))	18. Distribution Statement
Magnetic Suspension Aerodynamics Bulbous Base Cones	Unclassified - Unlimited

19. Security Classif. (of this report)	20. Security Classif. (of this page)	21. No. of Pages	22. Price*
Unclassified	Unclassified	63	$3.00

*For sale by the National Technical Information Service, Springfield, Virginia 22151

FOREWORD

This work was performed at the Aerophysics Laboratory, Massachusetts Institute of Technology, Cambridge, Massachusetts. The work was sponsored by the Full-Scale Research Division, NASA Langley Research Center, Hampton, Virginia, under contract NAS1-8658. This contract was monitored by Mr. Harleth Wiley, of the NASA Langley Vehicle Dynamics Section. Overall supervision of this study was provided by Professor Eugene E. Covert, of the M.I.T. Aerophysics Laboratory, in the capacity of Principal Investigator. This report covers work performed during the period from November 1969 to November 1970.

TABLE OF CONTENTS

LIST OF SYMBOLS

C_D	Drag coefficient = Drag/q$(\frac{\pi D^2}{4})$
C_L	Lift coefficient = Lift/q$(\frac{\pi D^2}{4})$
C_M	Moment coefficient = Moment/q$(\frac{\pi D^3}{4})$ (referred to model nose)
D	Cone forebody base diameter
M	Mach number
Re_D	Reynolds number base on cone forebody base diameter
q	Dynamic pressure
X_{cp}	Center of pressure location measured from cone forebody base
α	Model angle of attack

SUBSONIC AND SUPERSONIC STATIC AERODYNAMIC CHARACTERISTICS OF A FAMILY OF BULBOUS BASE CONES MEASURED WITH A MAGNETIC SUSPENSION AND BALANCE SYSTEM

By M. Vlajinac, T. Stephens, G. Gilliam, N. Pertsas
Massachusetts Institute of Technology

SUMMARY

Aerodynamic tests were conducted on a blunted 6° half angle cone forebody with a series of bulbous bases. Static force and moment data were obtained both at subsonic and supersonic speeds using the M.I.T.-N.A.S.A. prototype magnetic suspension and balance system.

The subsonic static data obtained on these configurations in some cases showed anomalous variation of the aerodynamic coefficients with angle of attack, particularly near zero. Also, under some conditions, hysteresis-type variation of the force and moment coefficients was observed, and was usually associated with appreciable unsteady aerodynamic loading of the model. A substantial change in the magnitude of the force and moment coefficients was observed after addition to the forebody of a circumferential boundary layer trip wire.

Tests were conducted to evaluate the effect of a dummy sting in the vicinity of the model base. The results show a pronounced decrease in the measured drag coefficient due to the presence of the sting.

The anomalous behavior of the subsonic aerodynamic characteristics is believed to be caused by irregular separation on the bulbous bases. The behavior, which exhibits both non-linearity and hysteresis, can have a significant effect on the stability of such configurations. Since separation appears to be very sensitive to the base flow process, it is concluded that freedom from support interference is desirable for this class of models.

INTRODUCTION

The static and dynamic characteristics of entry-type configurations are often affected by flow separation on the

body base (ref. 1). In some cases, the flow separation can cause negative damping of the body motion, or energy extraction from the flow, leading to dynamic instability. In addition to this, the location of the separation point can be "path dependent" causing a hysteresis behavior in the static coefficients as well as affecting the damping characteristics of the body. Wind tunnel tests on bulbous base cone configurations using conventional sting support for the models have shown the measured aerodynamic data to be strongly affected by sting interference on the surrounding flow (ref. 1,2). A practical method for obtaining interference-free aerodynamic data is by the use of a magnetic suspension and balance system. Development of such systems have been carried on at the M.I.T. Aerophysics Laboratory.*

APPARATUS

1. Magnetic Balance Description. - The magnetic balance used in these tests is described in detail in Ref. 3. The balance is presently capable of magnetically suspending a variety of ferromagnetic model geometries and measuring five components of force and moment on the model. (Rolling moments are not measured.) The forces and moments on the model are computed from the measured magnet coil currents required to balance the aerodynamic and gravity loads. The measured magnet currents, tunnel conditions and model position data are processed by a computer program which reduces the data to aerodynamic coefficient form. The data reduction

---

*The original development work at M.I.T. was sponsored by the Aerospace Research Laboratories, Wright-Patterson A.F.B., and a working system, which is still in use, was built. Further development work was sponsored by the NASA-Langley Research Center, and an improved magnetic suspension system was built. This system is referred to as the M.I.T.-N.A.S.A. Prototype Magnetic Suspension and Balance System.

techniques developed for this balance are discussed in detail in Ref. 4.

2. Supersonic Wind Tunnel. - Tests at supersonic speeds on the bulbous base cones were conducted in the M.I.T. Aerophysics Laboratory Gas Dynamic Facility. This facility is a continuous flow, open jet tunnel with several optional nozzle and diffuser conditions. For these tests, a M = 4.23, 3" x 4" nozzle was used. Tunnel stagnation temperature is controllable between approximately 200°F and 1000°F, and stagnation pressure between approximately 8 psia and 100 psia.

3. Subsonic Wind Tunnel. - The subsonic wind tunnel used in these tests was designed for use in conjunction with the magnetic balance system described earlier (ref. 3). It is an open circuit, closed jet tunnel with intake open to the test room. A continuous variation in velocity from 0 to 550 ft/sec can be obtained at the test section. This corresponds to a maximum dynamic pressure of 2.5 psi and freestream Reynolds number of 3.5×10^6/ft. The test section is octagonal, with an inside dimension of 6 1/4 inches.

4. Model Description. - The model used in these tests consisted of a 6° half angle blunt cone forebody with four different base configurations. The model configurations are shown in Figure 1. The cone forebody was machined from as-received Armco magnetic ingot iron. The bulbous base inserts were machined from cured epoxy and cemented into the base cavity in the forebody. Several identical forebodies and duplicates of each base insert were provided. Inserts have radii of 0.1, 0.5 and 1.25 times the forebody base diameter. These inserts are identified as Base 2, 3 and 4, respectively. The forebody alone (no insert) is designated as having Base 1. The forebody nose bluntness ratio (nose radius/forebody base radius) is 0.3. The hole in the model bases is for the purpose of testing the models with a dummy sting and obtaining sting interference data.

DESCRIPTION OF TESTS

1. Supersonic Tests. - Wind tunnel tests were conducted on the family of bulbous base cones to obtain static force and moment coefficients at Mach 4.23.* The nominal tunnel conditions throughout these tests were a stagnation absolute pressure of 25.0 psi, and a stagnation temperature of 300°F. Data were obtained on these models over an angle of attack range from -4° to +8° in nominal increments of 2°.

2. Data Acquisition. - The static forces and moments were obtained by measuring the magnet coil currents required to balance gravity and aerodynamic loads on the models. The magnet currents were measured with an integrating digital voltmeter. Integration (averaging) period for each current measurement was 10 seconds. The 10 second sampling attenuates the effects of ripple and noise and provides an accurate average of the coil current from which the steady state loads on the model can be obtained. Voltmeter readings were recorded with a digital printer.

The model position with respect to the wind tunnel axis was visually monitored and set with three transits. The model absolute position and orientation were measured to the following estimated accuracy:

Translations (lift, drag, slip): ±0.001 in.

Angles (pitch, yaw): ±0.1°.

---

*Attempts were made to measure the effect of a dummy sting on the measured coefficients in the course of the supersonic tests. However, the dummy sting apparently interfered with the tunnel starting process to such a degree that controlled suspension of the model was lost for all starts that were attempted with the sting present. In all cases, control was lost in the side force channel. This channel has the lowest power capability and, consequently, the poorest transient response. Blocking tests, however, showed that the model-sting combination would not block the tunnel.

The procedures used for each data point were the following:

1. The desired model position and orientation with respect to the tunnel were indexed on the transits. The model was then translated and rotated to this position with the magnetic balance position control (see ref. 3).

2. The wind tunnel stagnation pressure and temperature were recorded.

3. The six magnet currents were sampled for 10 seconds each and recorded.

4. The model position was checked to insure no change in position had occurred.

5. The transits were indexed for the next model position and the procedure returned to step 1.

A similar procedure as outlined above was repeated wind-off, with the omission of step 2, at each model position for which wind-on data had been taken. This provided the tare currents which are required in the data reduction process.

The resulting magnet currents, model position and tunnel conditions were processed by a computer program to reduce the data to aerodynamic coefficient form (see ref. 4).

3. Subsonic Tests. - Wind tunnel tests were conducted on the same bulbous base cone configurations at subsonic speeds. The nominal tunnel conditions for these tests were a dynamic pressure of 0.830 psi and a Mach number of 0.28. The nominal Reynolds number based on the cone forebody base diameter was 1.2×10^5. The angle of attack range was from -6° to +12° in nominal increments of 2°. Additional data points were taken in smaller angle increments where it was necessary to explore in greater detail anomalous variation of the coefficients with angle of attack.

Continuous plots of magnet currents versus angle of attack were made on an x-y plotter. The Electromagnetic Position Sensor (see ref. 3) signal was used to provide the model angle of attack in these plots. The model angle of attack was varied over the desired range by rotating the magnetic balance pitch position control. Since the position controls are effectively

decoupled, the resulting model motion was an angle of attack sweep in the pitch plane. The position sensor signal was then calibrated using the transits as an accurate angle reference. This technique proved useful particularly where non-linear and unsteady behavior of the forces and moments with angle of attack occurred. Discrete data points could obscure such behavior.

Static data at similar tunnel conditions were obtained with the four cone configurations with a circumferential boundary layer trip wire on the cone forebody surface. The trip consisted of a 0.017 in. diameter copper wire, in all cases located 1.75 in. from the base of the model forebody (see Fig. 1). The trip produced a turbulent boundary layer flow over the rear of the forebody, and turbulent separation from the base. These tests were performed since it is believed that the non-linear behavior of the static coefficients with angle of attack were primarily caused by laminar boundary layer separation from the model bases. In addition, the unsteady aerodynamic loads on the model were attributed to unsteadiness in the location of the separation point.

Attempts were made to obtain the aerodynamic damping-in-pitch coefficients for the bulbous base cones using a forced oscillation technique (ref. 4). The current amplitude required to force the model motion at its resonant frequency was more than 80 db below its off-resonance value, indicating a damping ratio of less than 4×10^{-5}. Tests performed on all four model configurations exhibited similar results. It became evident from these results that improvements in signal-to-noise ratio are required before this technique can be used successfully to measure small damping moments.

In addition to the above tests, static data on the base 3 configuration (see Fig. 1) were taken with a dummy sting attached to the wind tunnel walls and extending into the base cavity of the model. An illustration of the sting arrangement is shown in Figure 2. Since the sting was fixed to the tunnel

walls, the point of rotation of the model was about the model base and on the tunnel axis, thereby maintaining the sting centrally located in the base cavity. This point of rotation differed from that used in the remainder of the tests. The model was pitched in those cases about a point on the model surface, one base diameter from the base of the cone forebody, since the transits used for setting the model absolute position and orientation sight on the edge of the model and it is desirable to rotate the model about a point near the geometrical center of the balance.

RESULTS AND DISCUSSION

1. Supersonic Test Results. - The measured static coefficients and center of pressure location obtained at Mach 4.23 on the four cone models are shown in Table 1. The drag data were corrected for horizontal tunnel bouyancy, which was less than 0.3% of the measured drag at zero angle of attack.

The measured drag and lift coefficient for the four models versus angle of attack are shown in Figures 3 and 4, respectively. The figures show the addition of the bulbous bases to have little influence on the lift and drag of these models. The pitching moment coefficient, however, shown in Figure 5, indicates a slight stabilizing moment coefficient variation with angle of attack as the base size is increased. The angular offset in the lift and pitching moment curves (Figs. 4,5) are due to flow misalignment and curvature along the tunnel axis. The data was not corrected for this effect.

It is concluded that the bulbous bases have only a small effect on the static characteristics at Mach 4.23, with a slight increase in static stability with increasing base size.

2. Subsonic Test Results. - The measured static coefficients and center of pressure location for the bulbous based cones obtained at a nominal Mach number of 0.28 are shown in Table 2. The coefficients were corrected for tunnel blockage effects (ref. 5). The data represent tests both with and without the

use of the forebody boundary layer trip wire and is so designated in the tables. Results obtained with and without the boundary layer trip indicate that at the Reynolds number used in these tests (120,000), the flow near the model base was laminar or near transition in the untripped case. At the same Reynolds number, the addition of the boundary layer trip created a turbulent boundary layer over the rear portion of the model based on calculations in ref. 5.

The lift coefficient versus angle of attack for the model 1 configuration (flat base) is shown in Figure 6 for both the tripped and untripped cases. The boundary layer trip appears to have little effect on the lift coefficient. The drag coefficient versus angle of attack is shown in Figure 7 for the same model configuration. The effect of the trip is to increase the drag coefficient over the untripped case and is assumed to be due to both the drag of the trip and increased skin friction over the rear portion of the model, since the separation point is governed by the sharp corner at the base. The moment coefficient versus angle of attack for the Base 1 configuration is shown in Figure 8. The moment coefficient variation with angle of attack appears to be unaltered with the addition of the trip, though a tare angle of attack of approximately +0.3 degrees appears in the tripped case. Close examination of the lift and drag coefficient (Figs. 6, 7) indicates the presence of a tare angle of attack of similar magnitude in the case of the tripped model. This tare angle appears in the remaining data which were taken subsequent to the above tests and may be due to an angular misalignment of the pitch-monitoring transit with the test section flow direction.

The lift coefficient versus angle of attack for the Base 2 model configuration is shown in Figure 9. In contrast to the Base 1 results, an anomalous behavior of the lift coefficient near zero angle of attack is observed in the untripped case. In addition, the scatter in the data near zero angle of attack indicates unsteady aerodynamic forces on the model are present.

Though the forces were obtained by sampling the magnet currents for 10 seconds (see description of tests), the scatter in the repeat data indicates that the fluctuating forces are either random or have a considerably longer time constant than 10 seconds, or both. The unsteady aerodynamic loads on the model were verified by visually observing the model motion. The movement of a magnetically suspended model is the result of unsteady loads on the model whose magnitude and frequency are beyond the present control range of the magnet power amplifiers. If the unsteady loads on the model are of sufficient magnitude and frequency, a loss of magnetic model suspension occurs. This was exemplified during the Base 2 model tests with the addition of the boundary layer trip ring. Though the lift coefficient appears to be more linear with angle of attack than in the untripped case (Figure 9), no data could be taken at or near zero angle of attack due to model instability.

The drag coefficient versus angle of attack for the Base 2 model is shown in Figure 10. In the case of the untripped model, the measured drag coefficient has a non-repeatable character which appeared to be dependent on the sequence in which the data were taken. The various curves in Figure 10 for the untripped model are drawn to indicate the various curves that were generated during the data acquisition. This indicates the model base flow could be in transition and the location of the separation point on the base could be unsteady and dependent on the previous model history (path dependence or hysteresis). For the case of the tripped Base 2 configuration, the drag coefficient appears to be constant at a given angle of attack and does not exhibit a path-dependent behavior. However, in the case of the tripped model, the suspension instability caused by the fluctuating aerodynamic loads prevented data from being taken near zero angle of attack. The pitching moment variation with angle of attack for the Base 2 configuration is shown in Figure 11. Similar to the behavior of the lift and drag coefficient of this model with angle of attack, a non-linear and path dependent moment is

observed in the untripped case. The effect of the trip is seen to reduce the non-linearity of the moment coefficient with angle of attack, when compared with the untripped results.

The present results and observations during the tests of the Base 2 model led to the conclusion that in the case of laminar (or transition) base flow, the unsteady aerodynamic loads are a hysteresis type which, when averaged over 10 seconds, do not produce an "average" force which is independent of the direction in which the data are taken. In contrast to the laminar case, the unsteady aerodynamic loads with a turbulent base flow are such as to result in repeatable loads when averaged over 10 seconds and which are path independent. The associated model motion appeared to be of smaller magnitude, but higher frequency than in the laminar case. In the case of the turbulent base flow at and near zero angle of attack, the unsteady aerodynamic forces prevented data from being taken.

The model instability near zero angle of attack for the Base 3 model configuration was even more pronounced than in the previous model (Base 2). The lift coefficient versus angle of attack is shown in Figure 12. The untripped model exhibited a path dependence of the lift coefficient with angle of attack similar to the Base 2 drag coefficient behavior (Figure 10). Data points taken in a sequence (indicated by arrows) appear to follow separate paths at the lower angles of attack and coalesce at the higher angles of attack. Due to the instability near zero angle of attack, the wind tunnel flow had to be started with the model pitched above 4°. An unusual run was obtained with the model at 8° during the tunnel start. In this particular sequence, data were taken at continuously decreasing angles of attack to -1°; at which point the loss of magnetic suspension of the model occurred. The large positive values of lift coefficient at and near zero angle of attack should be noted as this reflects a "hysteresis"-type behavior.

A technique was used to obtain a continuous plot of lift coefficient versus angle of attack for the untripped Base 3

configuration in the angle of attack range from -2° to +4°. In this region, if a given average angle of attack is maintained, the unsteady aerodynamic loads produce model movements which diverge and cause loss of magnetic suspension control. Also, an accurate model angle of attack cannot be set with the transit. The technique employed to obtain an average lift force and angle of attack of the model involved pitching the model from positive to negative angles of attack at a sufficiently rapid rate (∿0.2°/sec) to prevent the unsteady aerodynamic loads on the model from amplifying the motion and causing loss of model suspension (see section on subsonic test description). The resulting curve (dashed line in Figure 12) represents the average lift coefficient versus average angle of attack since both the measured force (proportional to lift magnet current) and model position signals were low-pass filtered to remove the unsteady portion of the signal. The results appear to be hysteresis free since an identical curve was generated by sweeping the model angle from positive to negative and vice-versa. A tentative explanation for the absence of hysteresis is the effect of the superimposed unsteady motion, analogous to the demagnetization of a magnetic material by means of an alternating field. During this test, considerable model motion was observed as the model angle of attack went through zero. In contrast to this behavior, the curve indicating the hysteresis behavior of the lift coefficient with angle of attack (Fig. 12), the model motion viewed through the transits was imperceptible including the point at -1°, indicating a stable flow separation location.

The data obtained on the Base 3 model with the boundary layer trip ring are also shown in Figure 12. The lift coefficient in this case appears more linear with angle of attack than in the untripped case and did not exhibit a hysteresis behavior. The model instability near zero angle of attack, as in the Base 2 tests with the boundary layer tripped, prevented data from being obtained in this region.

The drag coefficient versus angle of attack for the Base

3 configuration is shown in Figure 13. In contrast to the results of the Base 1 and Base 2 results, the effect of the boundary layer trip is to reduce the drag coefficient over the untripped case. Since Base 3 is spherical, this effect is analogous to the classical result of drag reduction on a sphere by tripping the boundary layer and thereby shifting the separation point aft of the laminar case. Similar to the lift coefficient behavior for this model, the drag coefficient in the untripped case exhibited a path dependence. One curve obtained at negative angles of attack appears to tend towards the drag in the turbulent case, thus indicating the base flow could be in transition. The drag data corresponding to the run where a large lift coefficient was obtained at or near zero incidence (Fig. 12) appear to be nearly constant with angle of attack in this region.

The moment coefficient versus angle of attack for the Base 3 model is shown in Figure 14. The moment is referred to the nose of the model and thus reflects the anomalous behavior of the lift and drag coefficient for this model configuration.

The lift coefficient versus angle of attack for the Base 4 configuration is shown in Figure 15. The untripped model results indicate similar path-dependent behavior of the lift coefficient with angle of attack as in the Base 2 and Base 3 cases. The model instability at small angles of attack prevented data from being taken in these regions. Continuous data through zero angle of attack could not be obtained as with the Base 3 model due to the larger unsteady aerodynamic loads generated on this configuration. A marked reduction in lift was obtained with the addition of the boundary layer trip, accompanied by a marked improvement in model suspension stability. The increased model stability permitted data to be taken with the model at and near zero angle of attack.

The addition of the trip also produced a large reduction in the drag coefficient on the Base 4 model and is shown in Figure 16. The untripped data are seen to have the path-dependent behavior which characterized the results with the smaller bulbous bases.

3. Subsonic Sting Interference Results. - The static characteristics of the bulbous base cones have been shown to be affected by the nature of the flow over the rear portion of the model. Tests were performed on the Base 3 model to determine the effects of a dummy sting on the measured aerodynamic parameters and are described in an earlier section. The boundary layer trip ring was used on the model and identical tests were performed with and without the presence of the sting. The sting interference test results are shown in Table 3.

The effect of the sting on the lift coefficient versus angle of attack is shown in Figure 19. The presence of the dummy sting is seen to have a more pronounced effect at the larger angles of attack. Of particular interest was the marked increase in model stability observed near zero angle of attack with the sting present. This fact permitted data to be taken at and near zero angle of attack, whereas it had been impossible to obtain data in this region without the sting.

A considerable change in the drag coefficient was observed due to the addition of the dummy sting and is shown in Figure 20. These data again reflect the increased model stability with the addition of the sting permitting data to be taken at zero angle of attack.

A small discrepancy corresponding to a shift in angle of attack (0.8°) was observed when comparing the data obtained during the sting interference tests with the previously discussed results. The cause of this discrepancy is not fully understood at present and is believed to be related to the different rotation point of the model with respect to the tunnel walls, which was discussed earlier.

Comparison of the present data using a magnetic suspension system and data obtained in ref. 1 are shown in Figure 21. Though the Mach number in the two cases is approximately the same, the Reynolds number is an order of magnitude different. However, the agreement is good particularly in the non-linear region near zero angle of attack. The present results indicate

that the sting interference is sufficient to account for the disagreement between the two, and is in accord with the conclusions regarding model support interference on bulbous base cones in both references 1 and 2.

CONCLUSIONS AND RECOMMENDATIONS

Wind tunnel tests at both subsonic and supersonic speeds were conducted on a blunted 6° half angle cone with various bulbous bases using a magnetic suspension and balance system. From the results of these tests, the following were concluded:

1) At supersonic speeds (M=4.23), the addition of bulbous bases to a blunted 6° half angle cone has little effect on the measured static coefficients.

2) At subsonic speeds, the addition of bulbous bases to the cone forebody produces anomalous behavior of the static coefficients with angle of attack particularly where the base flow is laminar or in transition.

3) The addition of a boundary layer trip on the cone forebody increases the linearity of the lift and pitching moment coefficients with angle of attack and causes pronounced changes in the drag coefficient of the bulbous based cones. These changes are believed due to the separation characteristics on the base of the model.

4) The model motion observed at and near zero angle of attack is due to unsteady aerodynamic loads on the bulbous bases.

5) Hysteresis or path dependent behavior of static coefficients with angle of attack was observed on the bulbous base models with laminar or transition base flow. This phenomenon was not observed in the cases where the base flow was turbulent.

6) A marked change in static stability was observed with the largest bulbous base (Model 4) with turbulent flow over the model base. This was accompanied by a reduction in both the lift and drag coefficient compared to the laminar flow case.

7) Sting interference effects were measured and found to have considerable influence on the static coefficients. This is in agreement with conclusions regarding sting interference on bulbous base cones discussed elsewhere.

REFERENCES

1. Adcock, J.B., "Some Experimental Relations between the Static and Dynamic Stability Characteristics of Sting Mounted Cones with Bulbous Bases," Paper presented at the Third Technical Workshop on Dynamic-Stability Problems, Moffett Field, California, November 1968.

2. Ericsson, L.E. and Reding, J.P., "Aerodynamic Effects of Bulbous Bases," Lockheed Missiles & Space Co., Technical Report LMSC-4-17-68-4, November 1968.

3. Stephens, T., "Design, Construction, and Evaluation of a Magnetic Suspension and Balance System for Wind Tunnels," NASA CR-66903, November 1969.

4. Gilliam, G.D., "Data Reduction Techniques for Use with a Wind Tunnel Magnetic Suspension and Balance System," Massachusetts Institute of Technology, TR 167, available as NASA CR-111844, 1971.

5. Pankhurst, R.C. and Holder, D.W., Wind Tunnel Technique, Pitman & Sons, Ltd., 1952.

TABLE I. - SUPERSONIC DATA

Model Base #1

M=4.23

$\alpha°$	$Re_D x10^5$	C_D	C_L	C_M	Xcp/D
-4	0.7597	0.2020	-0.1133	0.3025	-1.0885
-4	0.7573	0.1982	-0.1098	0.2701	-1.2782
-2	0.7588	0.1868	-0.0554	0.1388	-1.2241
-1	0.7588	0.1831	-0.0322	0.0956	-0.7619
0	0.7612	0.1807	-0.0095	0.0491	1.6527
0	0.7588	0.1803	-0.0065	0.0297	1.0844
0	0.7597	0.1798	-0.0069	0.0233	-0.1012
0	0.7588	0.1795	-0.0049	0.0127	-0.1180
1	0.7576	0.1829	0.0187	-0.0262	-2.2673
2	0.7588	0.1878	0.0422	-0.0940	-1.5325
2	0.7597	0.1870	0.0424	-0.0948	-1.5291
3	0.7579	0.1945	0.0666	-0.1251	-1.8367
4	0.7579	0.2020	0.0931	-0.1896	-1.6944
4	0.7594	0.2014	0.0952	-0.2005	-1.6293
6	0.7594	0.2170	0.1483	-0.2808	-1.8174
6	0.7594	0.2189	0.1460	-0.2848	-1.7728
6	0.7691	0.2211	0.1520	-0.3065	-1.7093
8	0.7597	0.2460	0.2177	-0.4250	-1.7668
8	0.7483	0.2466	0.2222	-0.4461	-1.7145
9	0.7637	0.2571	0.2446	-0.4529	-1.8601

TABLE I. - SUPERSONIC DATA - Continued

Model Base #2

M=4.23

$\alpha°$	$Re_D x10^5$	C_D	C_L	C_M	Xcp/D
-2	0.7645	0.1877	-0.0588	0.1897	-0.5672
-1	0.7642	0.1820	-0.0336	0.1248	-0.0749
0	0.7199	0.1802	-0.0053	0.0266	-1.5306
0	0.7304	0.1804	-0.0073	0.0424	-2.3991
0	0.7603	0.1785	-0.0082	0.0527	-2.9993
0	0.7708	0.1782	-0.0067	0.0496	-3.9096
0	0.7648	0.1775	-0.0080	0.0550	-3.3985
0	0.7853	0.1770	-0.0071	0.0501	-3.5893
1	0.7653	0.1807	0.0160	-0.0012	-3.4074
2	0.7609	0.1872	0.0437	-0.0878	-1.7193
2	0.7651	0.1858	0.0397	-0.0609	-2.1506
3	0.7678	0.1943	0.0688	-0.1370	-1.7300
4	0.7612	0.2015	0.0939	-0.1718	-1.8786
4	0.7648	0.2016	0.0952	-0.1773	-1.8410
6	0.7696	0.2248	0.1550	-0.2925	-1.8214
7	0.7668	0.2346	0.1837	-0.3674	-1.7255
7	0.7785	0.2357	0.1882	-0.3981	-1.6208

TABLE I. - SUPERSONIC DATA - Continued

Model Base #3

M=4.23

$\alpha°$	$Re_D x10^5$	C_D	C_L	C_M	Xcp/D
-2	0.7693	0.1849	-0.0601	0.1775	-0.7996
-1	0.7676	0.1804	-0.0357	0.1216	-0.3390
0	0.7502	0.1800	-0.0064	0.0523	4.7346
0	0.7608	0.1776	-0.0055	0.0458	4.9277
0	0.7665	0.1785	-0.0062	0.0467	4.0368
0	0.7696	0.1785	-0.0077	0.0587	4.1722
1	0.7630	0.1810	0.0166	-0.0005	-3.4419
1	0.7725	0.1795	0.0177	-0.0091	-3.0295
2	0.7630	0.1860	0.0422	-0.0508	-2.4230
3	0.7633	0.1930	0.0701	-0.1265	-1.8885
4	0.7633	0.2010	0.0963	-0.1776	-1.8551
4	0.7696	0.2007	0.0963	-0.1795	-1.8371
6	0.7633	0.2214	0.1620	-0.3409	-1.6178
7	0.7590	0.2315	0.1925	-0.3901	-1.6889
7	0.7796	0.2337	0.1971	-0.4151	-1.6149

TABLE I. - SUPERSONIC DATA - Concluded

Model Base #4

M=4.23

$\alpha°$	$Re_D x10^5$	C_D	C_L	C_M	Xcp/D
-2	0.7693	0.1862	-0.0602	0.1908	-0.6076
-1	0.7716	0.1830	-0.0349	0.1361	0.1007
0	0.7516	0.1808	-0.0069	0.0678	6.3420
0	0.7687	0.1807	-0.0064	0.0621	6.2409
0	0.7696	0.1804	-0.0070	0.0664	6.0821
0	0.7624	0.1823	-0.0062	0.0623	6.5413
0	1.169	0.1760	-0.0066	0.0583	5.1412
1	0.7663	0.1828	0.0179	0.0181	-4.3232
2	0.7534	0.1881	0.0437	-0.0506	-2.4609
2	0.7728	0.1887	0.0468	-0.0715	-2.1294
3	0.7657	0.1956	0.0728	-0.1318	-1.8789
4	0.7648	0.2035	0.1022	-0.1942	-1.7964
4	0.7693	0.2039	0.1036	-0.2088	-1.6917
6	0.7717	0.2242	0.1676	-0.3411	-1.6735
7	0.7606	0.2359	0.2014	-0.4188	-1.6358
7	0.7766	0.2353	0.2012	-0.4169	-1.6414

TABLE II. - SUBSONIC DATA

Model Base #1

Untripped

$\alpha°$	M	$Re_D x10^6$	C_D	C_L	C_M	Xcp/D
-6	0.2812	0.1194	0.2845	-0.1844	0.3941	-1.6189
-4	0.2815	0.1196	0.2687	-0.1351	0.3015	-1.5032
-4	0.2812	0.1194	0.2695	-0.1347	0.3039	-1.4828
-2	0.2820	0.1198	0.2434	-0.0747	0.1469	-1.7000
-2	0.2816	0.1196	0.2459	-0.0773	0.1784	-1.3897
0	0.2782	0.1184	0.2391	0.0010	-0.0345	---
0	0.2817	0.1198	0.2349	-0.0041	0.0013	-3.1525
0	0.2816	0.1196	0.2346	-0.0068	0.0254	0.2521
1	0.2792	0.1189	0.2412	0.0352	-0.1083	-0.7192
2	0.2793	0.1189	0.2489	0.0645	-0.1367	-1.5974
2	0.2819	0.1199	0.2467	0.0635	-0.1282	-1.6888
3	0.2795	0.1190	0.2619	0.0974	-0.2204	-1.4816
4	0.2800	0.1192	0.2759	0.1255	-0.2654	-1.6303
4	0.2816	0.1198	0.2760	0.1262	-0.2753	-1.5709
6	0.2798	0.1191	0.3017	0.1733	-0.3683	-1.6609
6	0.2818	0.1198	0.3008	0.1725	-0.3638	-1.6759
8	0.2797	0.1191	0.3320	0.2219	-0.4752	-1.6803
8	0.2809	0.1195	0.3324	0.2226	-0.4934	-1.6173
10	0.2796	0.1190	0.3655	0.2695	-0.5985	-1.6476
10	0.2806	0.1194	0.3644	0.2679	-0.5736	-1.738
12	0.2797	0.1190	0.3975	0.3183	-0.6717	-1.7625

TABLE II. - SUBSONIC DATA - Continued

Model Base #1

Boundary Layer Tripped

$\alpha°$	M	$Re_D x10^6$	C_D	C_L	C_M	Xcp/D
-6	0.2836	0.1201	0.3192	-0.1869	0.4122	-1.5878
-6	0.2838	0.1201	0.3212	-0.1886	0.4412	-1.4724
-4	0.2838	0.1202	0.2969	-0.1387	0.3182	-1.4675
-2	0.2838	0.1202	0.2730	-0.0887	0.2026	-1.4046
-2	0.2841	0.1203	0.2705	-0.0863	0.1957	-1.4224
0	0.2838	0.1202	0.2479	-0.0114	0.0196	-1.7489
1	0.2842	0.1203	0.2534	0.0274	-0.0475	-1.9751
2	0.2837	0.1203	0.2716	0.0665	-0.1491	-1.5022
4	0.2829	0.1200	0.2986	0.1175	-0.2264	-1.8278
6	0.2826	0.1198	0.3245	0.1669	-0.3484	-1.7243
6	0.2839	0.1201	0.3264	0.1679	-0.3758	-1.5989
8	0.2820	0.1196	0.3493	0.2111	-0.4310	-1.7948
10	0.2818	0.1195	0.3779	0.2589	-0.5385	-1.7876
10	0.2839	0.1201	0.3777	0.2578	-0.5362	-1.7893
12	0.2831	0.1198	0.4176	0.3037	-0.6256	-1.8378

TABLE II. - SUBSONIC DATA - Continued

Model Base #2

Untripped

$\alpha°$	M	$Re_D x10^6$	C_D	C_L	C_M	Xcp/D
-6	0.2765	0.1172	0.2947	-0.1891	0.4182	-1.5572
-6	0.2777	0.1185	0.3047	-0.2046	0.4647	-1.4931
-4	0.2759	0.1171	0.2872	-0.1468	0.3654	-1.2729
-4	0.2774	0.1185	0.2964	-0.1600	0.3900	-1.3043
-4	0.2782	0.1186	0.2929	-0.1589	0.3833	-1.3259
-4	0.2785	0.1188	0.2956	-0.1614	0.3989	-1.2717
-4	0.2800	0.1187	0.2984	-0.1476	0.3631	-1.3075
-2	0.2772	0.1185	0.2865	-0.1186	0.3025	-1.1151
-2	0.2760	0.1171	0.2774	-0.1056	0.2564	-1.243
-2	0.2785	0.1188	0.2865	-0.1174	0.2937	-1.1611
-2	0.2808	0.1189	0.2896	-0.1111	0.3080	-0.9250
-2	0.2826	0.1196	0.2832	-0.0974	0.2081	-1.5263
-2	0.2527	0.1068	0.2832	-0.1023	0.2498	-1.2397
-1	0.2764	0.1172	0.2905	-0.0912	0.2608	-0.7591
-0.5	0.2765	0.1173	0.2934	-0.0792	0.2238	-0.7290
-0.5	0.2825	0.1196	0.2883	-0.0586	0.1227	-1.4590
0	0.2728	0.1161	0.2534	-0.0020	-0.0118	-9.5163
0	0.2771	0.1185	0.2636	-0.0109	-0.0173	-5.0544
0	0.2787	0.1189	0.2617	-0.0208	0.0566	-0.7470
0	0.2788	0.1189	0.2644	-0.0247	0.0689	-0.6728
0	0.2817	0.1192	0.2883	-0.0534	0.2403	1.0283
0	0.2789	0.1179	0.2625	-0.0055	0.0069	-2.2018
0	0.2789	0.1179	0.2808	-0.0031	0.0082	-0.8517
0.5	0.2823	0.1195	0.2877	-0.0121	0.0477	1.4994
1	0.2734	0.1163	0.2812	0.0707	-0.1863	-1.0048

TABLE II. - SUBSONIC DATA - Continued

Model Base #2

Untripped-Continued

$\alpha°$	M	$Re_D x10^6$	C_D	C_L	C_M	Xcp/D
1	0.2764	0.1173	0.2794	0.0739	-0.2049	-0.8599
1	0.2822	0.1195	0.2892	0.0545	-0.1921	-0.2411
1.5	0.2818	0.1193	0.2920	0.0730	-0.2013	-0.9704
2	0.2738	0.1164	0.2842	0.0910	-0.2135	-1.3508
2	0.2763	0.1173	0.2836	0.0941	-0.2206	-1.3452
2	0.2788	0.1190	0.2848	0.0920	-0.2323	-1.1868
2	0.2819	0.1193	0.2950	0.0819	-0.1723	-1.5983
3	0.2738	0.1164	0.2909	0.1156	-0.2737	-1.3738
3	0.2765	0.1173	0.2873	0.1138	-0.2790	-1.2994
4	0.2790	0.1190	0.2915	0.1317	-0.3034	-1.4679
6	0.2787	0.1189	0.3040	0.1760	-0.3917	-1.5734
6	0.2818	0.1193	0.3123	0.1700	-0.3715	-1.6254
7	0.2759	0.1171	0.3123	0.1996	-0.4197	-1.6905
8	0.2751	0.1168	0.3260	0.2248	-0.4798	-1.6770
8	0.2786	0.1188	0.3291	0.2247	-0.4913	-1.6360
10	0.2754	0.1170	0.3547	0.2714	-0.5810	-1.7008
10	0.2750	0.1168	0.3547	0.2703	-0.5598	-1.7600
10	0.2782	0.1186	0.3577	0.2713	-0.5800	-1.7062
10	0.2817	0.1192	0.3617	0.2599	-0.5365	-1.7846
12	0.2748	0.1167	0.3887	0.3227	-0.6718	-1.7731

TABLE II. - SUBSONIC DATA - Continued

Model Base #2

Boundary Layer Tripped

$\alpha°$	M	$Re_D x10^6$	C_D	C_L	C_M	Xcp/D
-6	0.2815	0.1189	0.3446	-0.1820	0.4081	-1.5873
-4	0.2815	0.1189	0.3265	-0.1310	0.3124	-1.4313
-2	0.2811	0.1188	0.3073	-0.0768	0.1669	-1.5605
-2	0.2815	0.1189	0.3108	-0.0794	0.2055	-1.1886
-1	0.2809	0.1188	0.2990	-0.0515	0.1382	-1.032
2	0.2803	0.1186	0.3023	0.0451	-0.0595	-2.3968
2	0.2820	0.1191	0.3015	0.0534	-0.0845	-2.1450
3	0.2820	0.1191	0.3131	0.0905	-0.1792	-1.7894
3	0.2808	0.1187	0.3124	0.0868	-0.1722	-1.7966
4	0.2803	0.1186	0.3225	0.1131	-0.2333	-1.7436
6	0.2799	0.1185	0.3445	0.1605	-0.3338	-1.7608
6	0.2827	0.1194	0.3455	0.1645	-0.3228	-1.8516
8	0.2795	0.1183	0.3666	0.2058	-0.4209	-1.8155
10	0.2788	0.1180	0.4007	0.2539	-0.5235	-1.8295
10	0.2827	0.1194	0.3993	0.2522	-0.5188	-1.8343
12	0.2783	0.1178	0.4451	0.3034	-0.6460	-1.8083

TABLE II. - SUBSONIC DATA - Continued

Model Base #3

Untripped

$\alpha°$	M	$Re_D x10^6$	C_D	C_L	C_M	Xcp/D
-7	0.2857	0.1181	0.3055	-0.2615	0.6332	-1.3339
-6	0.2860	0.1183	0.2987	-0.2378	0.5981	-1.2336
-6	0.2857	0.1181	0.2989	-0.2361	0.5915	-1.2443
-4	0.2860	0.1184	0.2901	-0.2065	0.5561	-1.009
-4	0.2862	0.1183	0.2888	-0.2055	0.5620	-0.9716
-3	0.2865	0.1184	0.2865	-0.1922	0.5482	-0.8179
-3	0.2863	0.1184	0.2856	-0.1916	0.5413	-0.8431
-2.5	0.2863	0.1184	0.2711	-0.1570	0.4633	-0.7201
-2	0.2865	0.1186	0.2517	-0.1195	0.3289	-0.9011
3.5	0.2867	0.1185	0.2980	0.1735	-0.4525	-1.1024
4	0.2861	0.1183	0.2956	0.1750	-0.4699	-1.0595
4	0.2862	0.1183	0.2952	0.1756	-0.4745	-1.0430
4	0.2861	0.1185	0.2961	0.1734	0.4660	-1.0612
4	0.2843	0.1173	0.3106	0.2070	-0.5951	-0.8593
5	0.2843	0.1172	0.3163	0.2191	-0.5694	-1.1510
5	0.2859	0.1185	0.3003	0.1871	-0.4333	-1.4297
6	0.2847	0.1174	0.3158	0.2241	-0.5350	-1.3762
6	0.2897	0.1200	0.3027	0.2048	-0.4875	-1.3958
6	0.2856	0.1183	0.3043	0.2026	-0.4715	-1.4464
6	0.2858	0.1184	0.3043	0.2034	-0.4686	-1.4656
7	0.2845	0.1172	0.3212	0.2388	-0.5742	-1.3884
8	0.2889	0.1196	0.3209	0.2485	-0.5592	-1.5444
10	0.2889	0.1197	0.3527	0.3047	-0.6889	-1.5612
10	0.2861	0.1182	0.3481	0.2969	-0.6104	-1.7377
10	0.2861	0.1182	0.3533	0.3055	-0.6912	-1.5593
12	0.2891	0.1191	0.3895	0.3624	-0.8409	-1.5363
12	0.2882	0.1195	0.3880	0.3609	-0.8207	-1.5752

TABLE II. - SUBSONIC DATA - Continued

Model Base #3

Untripped-Continued

$\alpha°$	M	$Re_D x10^6$	C_D	C_L	C_M	Xcp/D
8	0.2744	0.1140	0.3307	0.2727	-0.6416	-1.4379
6	0.2741	0.1139	0.3187	0.2390	-0.5922	-1.2828
5	0.2751	0.1142	0.3120	0.2257	-0.5879	-1.1349
4	0.2753	0.1143	0.3122	0.2238	-0.6330	-0.8845
3	0.2753	0.1143	0.3108	0.2164	-0.6450	-0.6918
2	0.2758	0.1145	0.3094	0.2094	-0.6534	-0.4984
1	0.2758	0.1145	0.3112	0.2011	-0.6637	-0.2542
0	0.2758	0.1145	0.3068	0.1975	-0.6782	-0.0335
-1	0.2758	0.1145	0.3044	0.1494	-0.6249	0.8710
-2.9	0.2774	0.1151	0.2886	-0.1861	0.5343	-0.8023
-4	0.2771	0.1150	0.2918	-0.2025	0.5501	-0.9935
-5	0.2766	0.1148	0.2970	-0.2200	0.5673	-1.1521

TABLE II. - SUBSONIC DATA - Continued

Model Base #3

Boundary Layer Tripped

$\alpha°$	M	$Re_D x10^6$	C_D	C_L	C_M	Xcp/D
-5	0.2795	0.1185	0.2497	-0.1874	0.4390	-1.3618
-4	0.2794	0.1184	0.2344	-0.1634	0.3956	-1.2623
-4	0.2810	0.1191	0.2346	-0.1641	0.3940	-1.2787
-3	0.2794	0.1185	0.2235	-0.1426	0.3839	-0.9766
-2	0.2793	0.1184	0.2117	-0.1199	0.3646	-0.6006
-2	0.2805	0.1189	0.2108	-0.1159	0.3254	-0.8271
2	0.2790	0.1183	0.2068	0.0879	-0.2232	-1.1198
2	0.2802	0.1188	0.2063	0.0888	-0.2299	-1.0711
2	0.2800	0.1166	0.2189	0.0930	-0.2741	-0.7423
3	0.2785	0.1182	0.2170	0.1107	-0.2733	-1.2260
4	0.2796	0.1182	0.2264	0.1255	-0.2722	-1.5369
4	0.2784	0.1181	0.2272	0.1300	-0.2940	-1.4470
4	0.2803	0.1189	0.2265	0.1297	-0.2817	-1.5277
4	0.2794	0.1163	0.2409	0.1368	-0.3718	-1.0423
4	0.2799	0.1165	0.2378	0.1340	-0.3281	-1.2838
5	0.2783	0.1182	0.2421	0.1536	-0.3148	-1.6591
6	0.2785	0.1178	--	0.1786	-0.3709	-1.6977
6	0.2792	0.1181	0.2604	0.1726	-0.3607	-1.6540
6	0.2805	0.1189	0.2602	0.1761	-0.3676	-1.6507
6	0.2798	0.1165	0.2633	0.1717	-0.3732	-1.5849
8	0.2793	0.1181	0.2937	0.2112	-0.4161	-1.8034
8	0.2799	0.1165	0.2934	0.2085	-0.4414	-1.6828
10	0.2780	0.1176	0.3163	0.2366	-0.3637	-2.2044
10	0.2811	0.1192	0.3227	0.2435	-0.4215	-2.0430
12	0.2761	0.1168	0.3536	0.2649	-0.4693	-2.0567
12	0.2811	0.1191	0.3501	0.2652	-0.4522	-2.1061

TABLE II. - SUBSONIC DATA - Continued

Model Base #4

Untripped

$\alpha°$	M	$Re_D x10^6$	C_D	C_L	C_M	Xcp/D
-8	0.2797	0.1161	0.2473	-0.2142	0.4016	-1.8382
-7.5	0.2771	0.1147	0.2516	-0.2171	0.4522	-1.6448
-6	0.2798	0.1161	0.2371	-0.1753	0.3753	-1.5829
-6	0.2799	0.1162	0.2383	-0.1748	0.3944	-1.4831
-6	0.2772	0.1148	0.2454	-0.1932	0.4633	-1.3405
-5	0.2773	0.1149	0.2411	-0.1805	0.4544	-1.2047
-4	0.2802	0.1161	0.2301	-0.1556	0.3777	-1.2623
-4	0.2800	0.1164	0.2295	-0.1556	0.3808	-1.2430
-4	0.2774	0.1149	0.2363	-0.1702	0.4463	-1.0717
-3	0.2801	0.1160	0.2280	-0.1491	0.4062	-0.9415
-3	0.2800	0.1164	0.2281	-0.1479	0.4064	-0.9219
-3	0.2772	0.1148	0.2352	-0.1616	0.4609	-0.8140
-2	0.2800	0.1164	0.2191	-0.1000	0.2944	-0.7226
3	0.2798	0.1161	0.2304	0.1169	-0.3028	-1.1177
3	0.2805	0.1162	0.2292	0.1153	-0.2885	-1.1988
3	0.2774	0.1149	0.2400	0.1503	-0.3947	-1.0412
4	0.2831	0.1173	0.2479	0.1744	-0.4637	-1.0429
4	0.2796	0.1160	0.2362	0.1864	-0.4243	-1.3717
4	0.2793	0.1158	0.2381	0.1500	-0.3607	-1.2974
4	0.2773	0.1149	0.2426	0.1610	-0.3857	-1.2956
5	0.2793	0.1157	0.2413	0.1593	-0.3540	-1.4977
5	0.2772	0.1149	0.2448	0.1679	-0.3702	-1.5047
6	0.2829	0.1172	0.2550	0.1927	-0.4227	-1.5309
6	0.2846	0.1178	0.2478	0.1869	-0.3816	-1.6654
6	0.2802	0.1161	0.2424	0.1673	-0.3284	-1.7544
6	0.2770	0.1147	0.2493	0.1786	-0.3705	-1.6481

TABLE II. - SUBSONIC DATA - Continued

Model Base #4

Untripped-Continued

$\alpha°$	M	$Re_D x10^6$	C_D	C_L	C_M	Xcp/D
7.8	0.2831	0.1173	0.2646	0.2187	-0.4486	-1.6917
8	0.2838	0.1175	0.2648	0.2211	-0.4496	-1.7102
8	0.2849	0.1180	0.2588	0.2238	-0.4342	-1.7819
8	0.2769	0.1148	0.2597	0.2099	-0.4041	-1.8115
10	0.2832	0.1172	0.2819	0.2565	-0.4848	-1.8600
10	0.2764	0.1146	0.2771	0.2525	-0.4448	-1.9688
12	0.2831	0.1172	0.3021	0.3016	-0.5291	-1.9886

TABLE II. - SUBSONIC DATA - Concluded

Model Base #4

Boundary Layer Tripped

$\alpha°$	M	$Re_D x10^6$	C_D	C_L	C_M	Xcp/D
-8	0.2826	0.1192	0.1195	-0.0721	-0.1931	-5.6624
-6	0.2827	0.1193	0.1144	-0.0567	-0.1058	-5.0160
-4	0.2825	0.1192	0.1092	-0.0438	-0.0670	-4.7734
-4	0.2827	0.1193	0.1092	-0.0432	-0.0638	-4.7257
-2	0.2829	0.1193	0.1056	-0.0318	0.0062	-3.2919
-2	0.2825	0.1193	0.1059	-0.0324	0.0134	-3.0973
-1	0.2824	0.1192	0.1051	-0.0254	0.0478	-1.7116
0	0.2826	0.1193	0.1040	-0.0103	0.0413	0.5310
0	0.2826	0.1192	0.1042	-0.0126	0.0405	-0.2613
1	0.2825	0.1192	0.1047	0.0208	-0.0331	-2.0053
1	0.2827	0.1192	0.1043	0.0230	-0.0511	-1.4110
2	0.2824	0.1193	0.1057	0.0301	0.0057	-3.6352
4	0.2825	0.1193	0.1086	0.0440	0.0665	-4.7597
4	0.2827	0.1192	0.1085	0.0442	0.0688	-4.7997
6	0.2823	0.1192	0.1124	0.0565	0.1296	-5.3758
8	0.2824	0.1193	0.1174	0.0707	0.1765	-5.5110
8	0.2827	0.1192	0.1177	0.0703	0.1893	-5.6688
10	0.2822	0.1192	0.1274	0.0897	0.2316	-5.5648
12	0.2814	0.1188	0.1411	0.1146	0.2587	-5.2963
12	0.2831	0.1194	0.1403	0.1136	0.2694	-5.3878

TABLE III. - SUBSONIC STING INTERFERENCE DATA

Model Base #3

Boundary Layer Tripped
Without Sting

$\alpha°$	M	$Re_D x10^6$	C_D	C_L	C_M	Xcp/D
-6	0.2790	0.1156	0.2715	-0.1784	0.4136	-1.4580
-4	0.2794	0.1158	0.2404	-0.1338	0.3035	-1.4477
-4	0.2794	0.1158	0.2463	-0.1331	0.3197	-1.3360
-2	0.2799	0.1160	0.2177	-0.0795	0.2125	-1.0276
-2	0.2794	0.1158	0.2223	-0.0719	0.1862	-1.1293
1	0.2830	0.1173	0.2175	0.0860	-0.2491	-0.6911
1	0.2796	0.1158	0.2168	0.0849	-0.2586	-0.5522
2	0.2787	0.1155	0.2267	0.1082	-0.2769	-1.0814
3	0.2808	0.1163	0.2409	0.1262	-0.3077	-1.2482
3	0.2806	0.1163	0.2384	0.1317	-0.3230	-1.2248
3	0.2806	0.1163	0.2390	0.1293	-0.3149	-1.2435
4	0.2819	0.1168	0.2540	0.1499	-0.3581	-1.3270
4	0.2818	0.1168	0.2533	0.1480	-0.3434	-1.3909
4	0.2797	0.1159	0.2546	0.1584	-0.3652	-1.3900
6	0.2819	0.1168	0.2867	0.1937	-0.4539	-1.4290
6	0.2801	0.1161	0.2893	0.2028	-0.4917	-1.3475
8	0.2823	0.1170	0.3154	0.2263	-0.4856	-1.6558
8	0.2799	0.1160	0.3147	0.2292	-0.5162	-1.5607
10	0.2818	0.1168	0.3436	0.2517	-0.5607	-1.6444
10	0.2821	0.1169	0.3391	0.2498	-0.5194	-1.7637
11	0.2821	0.1169	0.3559	0.2630	-0.5538	-1.7692
11	0.2796	0.1159	0.3556	0.2636	-0.5637	-1.7417
12	0.2818	0.1168	0.3722	0.2793	-0.5884	-1.7893
12	0.2819	0.1168	0.3724	0.2776	-0.5871	-1.7851
12	0.2805	0.1162	0.3637	0.2738	-0.5299	-1.9245

TABLE III. - SUBSONIC STING INTERFERENCE DATA

Model Base #3

Boundary Layer Tripped
With Sting

$\alpha°$	M	$Re_D 10^6$	C_D	C_L	C_M	Xcp/D
-6	0.2808	0.1157	0.2359	-0.1776	0.4142	-1.4097
-4	0.2808	0.1157	0.2167	-0.1372	0.3085	-1.4381
-4	0.2808	0.1157	0.2157	-0.1365	0.3300	-1.2846
-3	0.2808	0.1157	0.2089	-0.1136	0.2784	-1.2288
-2	0.2807	0.1157	0.2018	-0.0859	0.2476	-0.8022
-2	0.2808	0.1157	0.2003	-0.0831	0.2205	-1.0186
-1	0.2805	0.1156	0.1971	-0.0335	0.0917	-0.9881
0	0.2802	0.1154	0.1970	0.0132	-0.0443	-0.0974
1	0.2802	0.1154	0.2014	0.0714	-0.1956	-0.8566
2	0.2802	0.1154	0.2100	0.1095	-0.2978	-0.9168
2	0.2808	0.1157	0.2098	0.1099	-0.2840	-1.0434
3	0.2802	0.1154	0.2182	0.1352	-0.3355	-1.1771
3	0.2800	0.1158	0.2207	0.1319	-0.3197	-1.2364
4	0.2811	0.1158	0.2260	0.1566	-0.3642	-1.3499
4	0.2777	0.1144	0.2297	0.1599	-0.4007	-1.1844
4	0.2799	0.1153	0.2290	0.1594	-0.3881	-1.2501
4	0.2790	0.1154	0.2277	0.1550	-0.3520	-1.4033
6	0.2820	0.1162	0.2499	0.2005	-0.4644	-1.4079
6	0.2784	0.1147	0.2521	0.2000	-0.4675	-1.3921
6	0.2799	0.1153	0.2514	0.2004	-0.4639	-1.4107
6	0.2794	0.1155	0.2506	0.1961	-0.4284	-1.5308
8	0.2815	0.1160	0.2805	0.2420	-0.5289	-1.5695
8	0.2791	0.1150	0.2818	0.2388	-0.5150	-1.5994
8	0.2795	0.1152	0.2779	0.2365	-0.4749	-1.7274
8	0.2797	0.1156	0.2821	0.2393	-0.5335	-1.5365
10	0.2786	0.1148	0.3084	0.2687	-0.5915	-1.6085
10	0.2791	0.1150	0.3060	0.2663	-0.5560	-1.7045
10	0.2800	0.1158	0.3058	0.2687	-0.5613	-1.7009
10	0.2815	0.1160	0.3030	0.2665	-0.5469	-1.7316
12	0.2788	0.1149	0.3338	0.2979	-0.5899	-1.8327

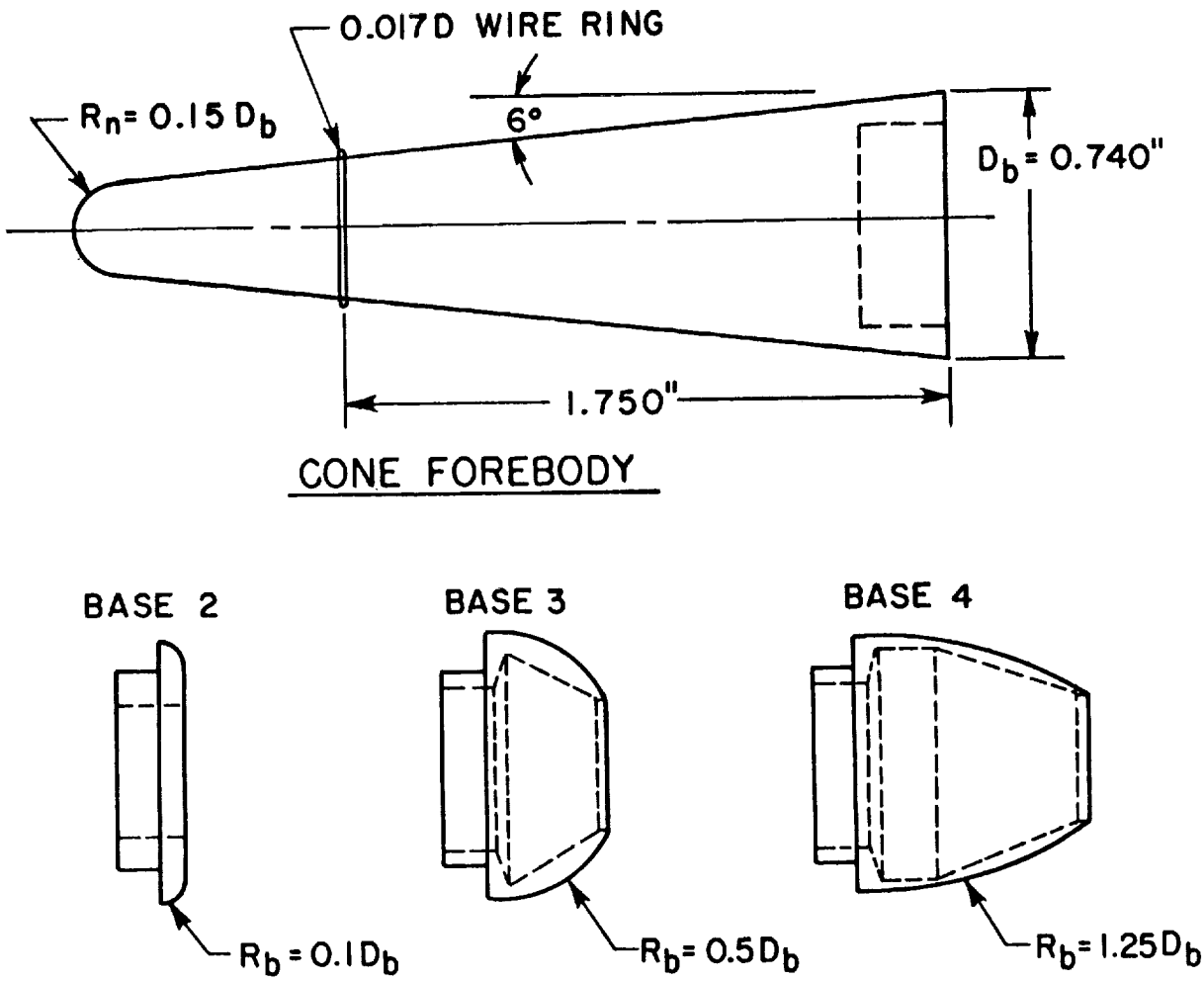

Figure 1. Bulbous Base Cone Models

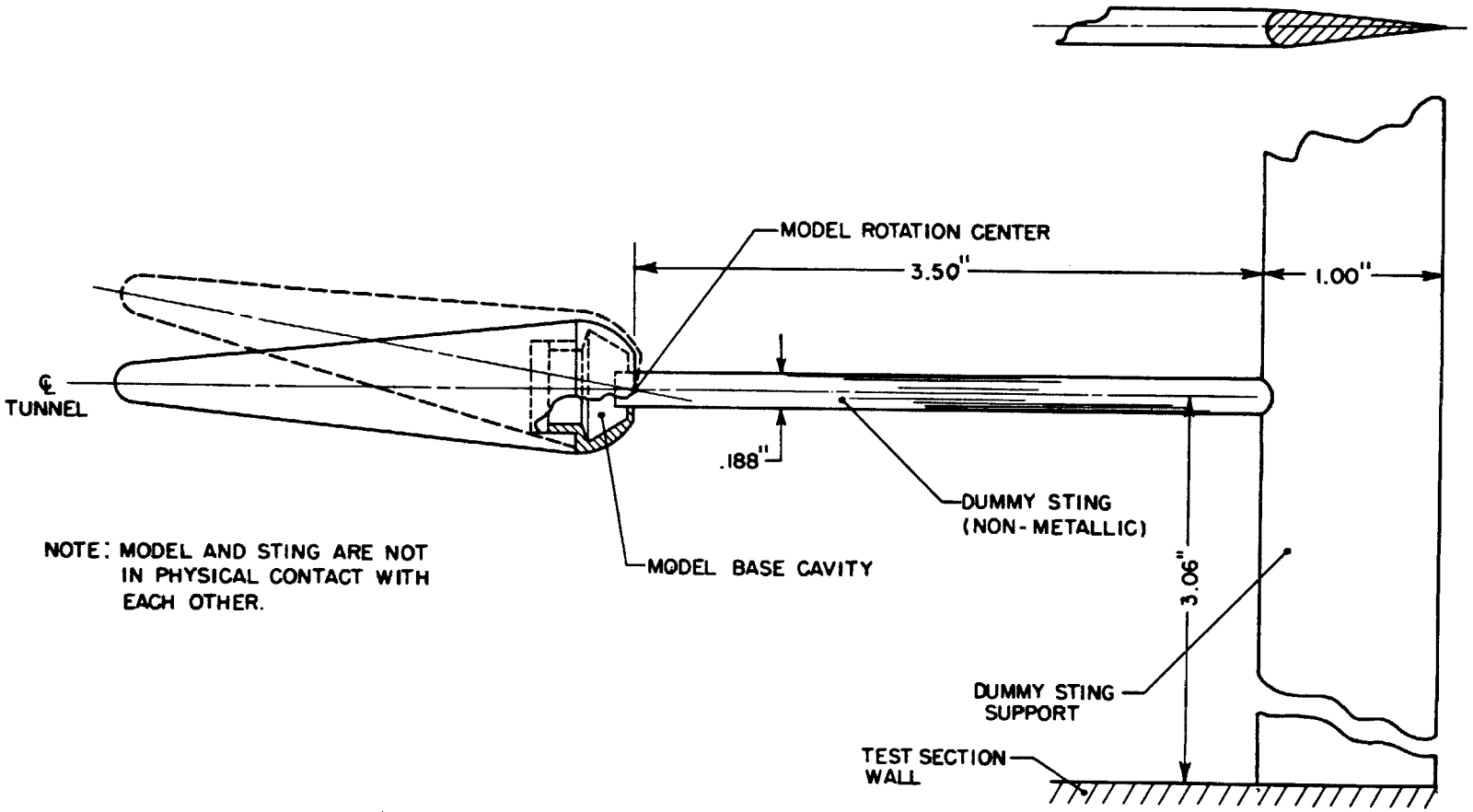

Figure 2. Sting Interference Test Arrangement

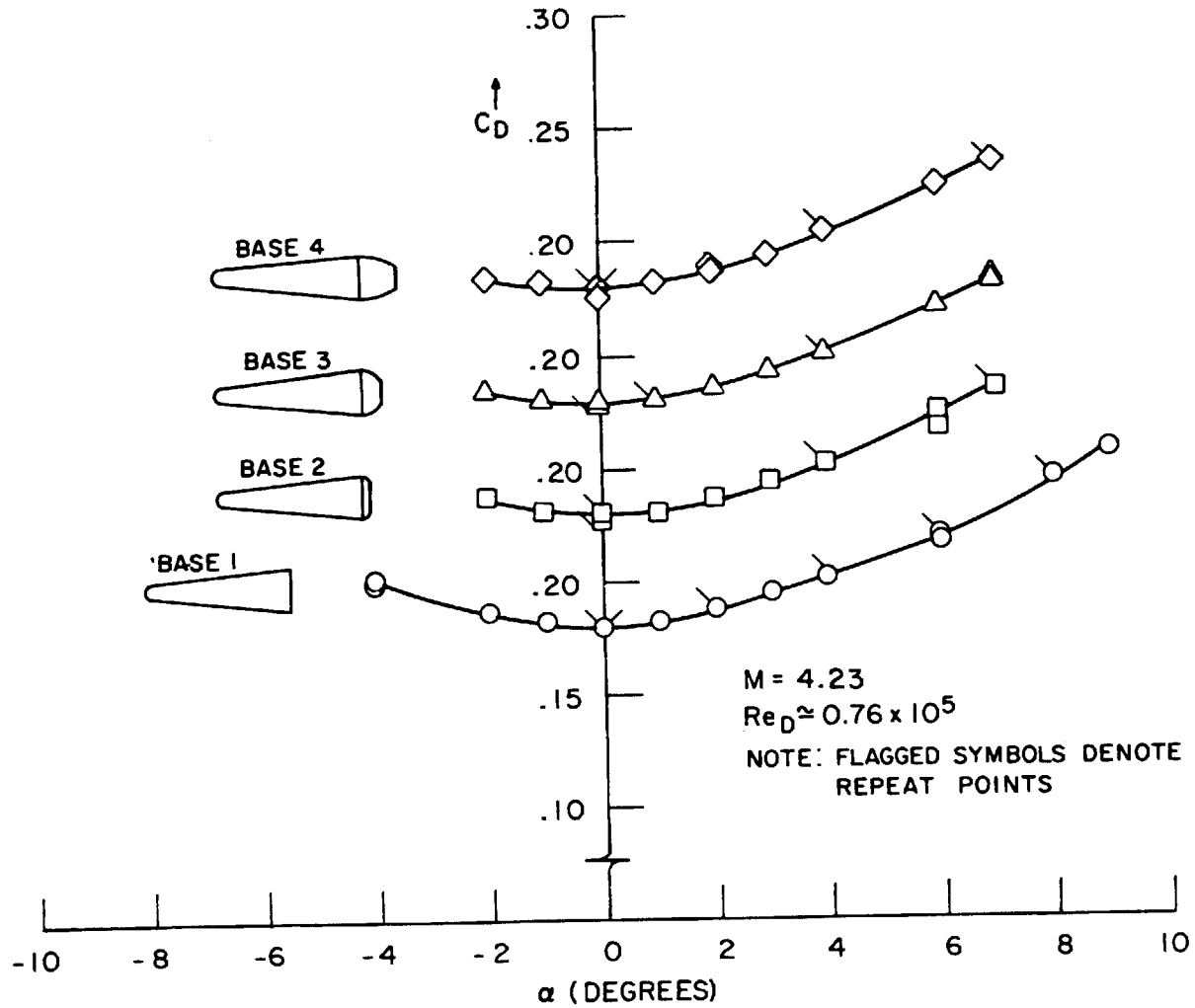

Figure 3. Supersonic Drag Coefficient versus Angle of Attack (All Models)

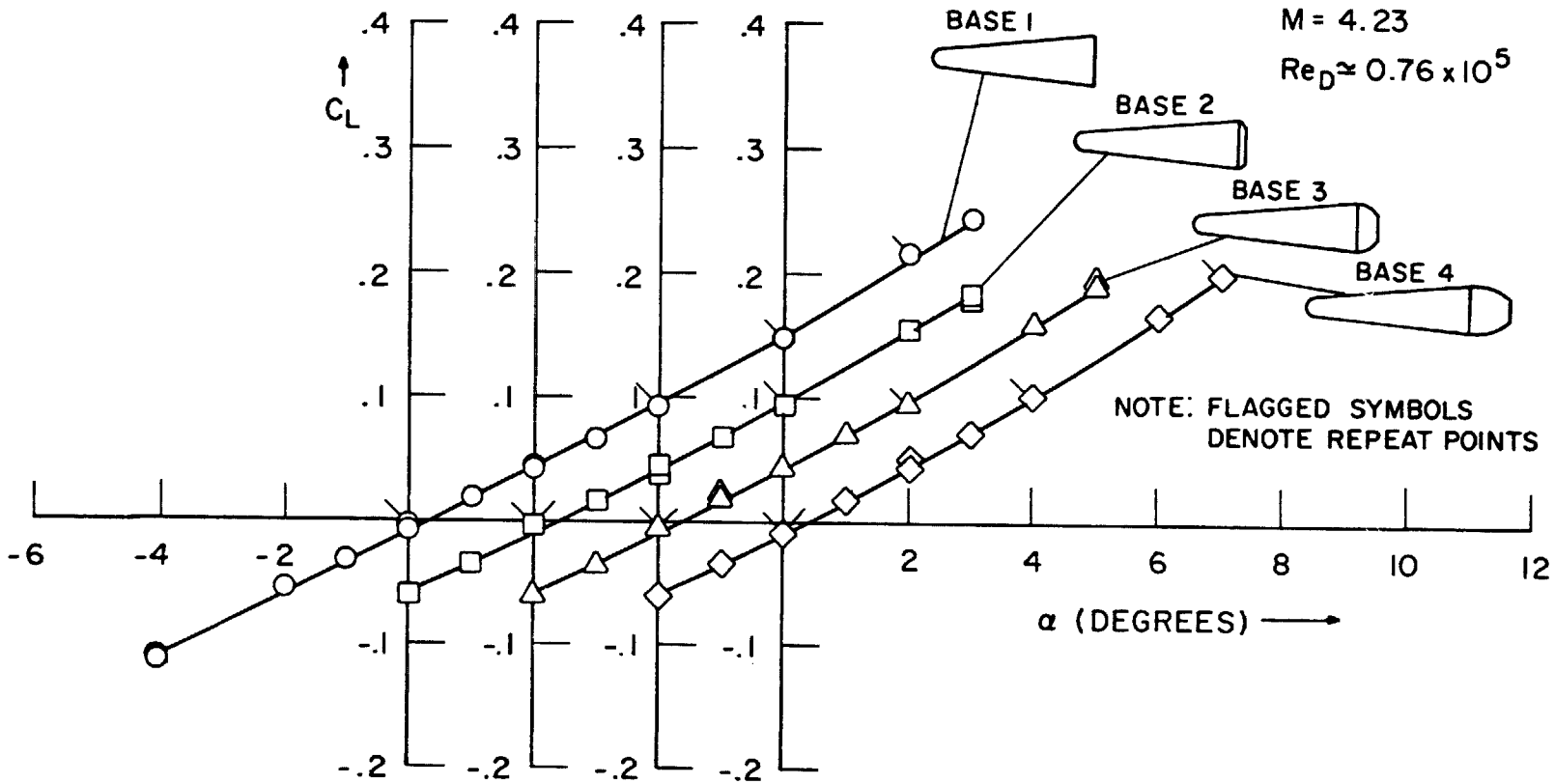

Figure 4. Supersonic Lift Coefficient versus Angle of Attack (All Models)

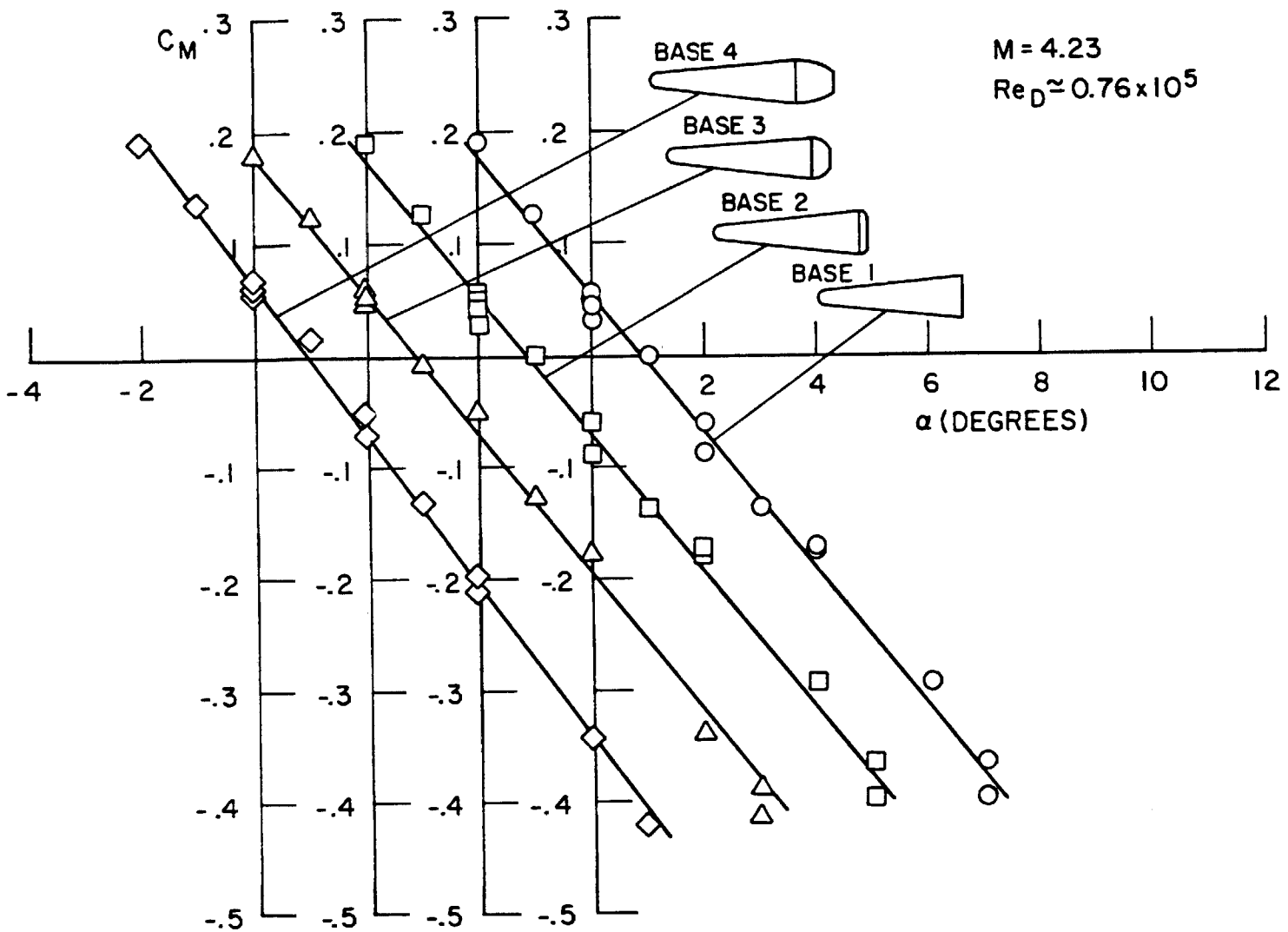

Figure 5. Supersonic Pitching Moment Coefficient versus Angle of Attack (All Models)

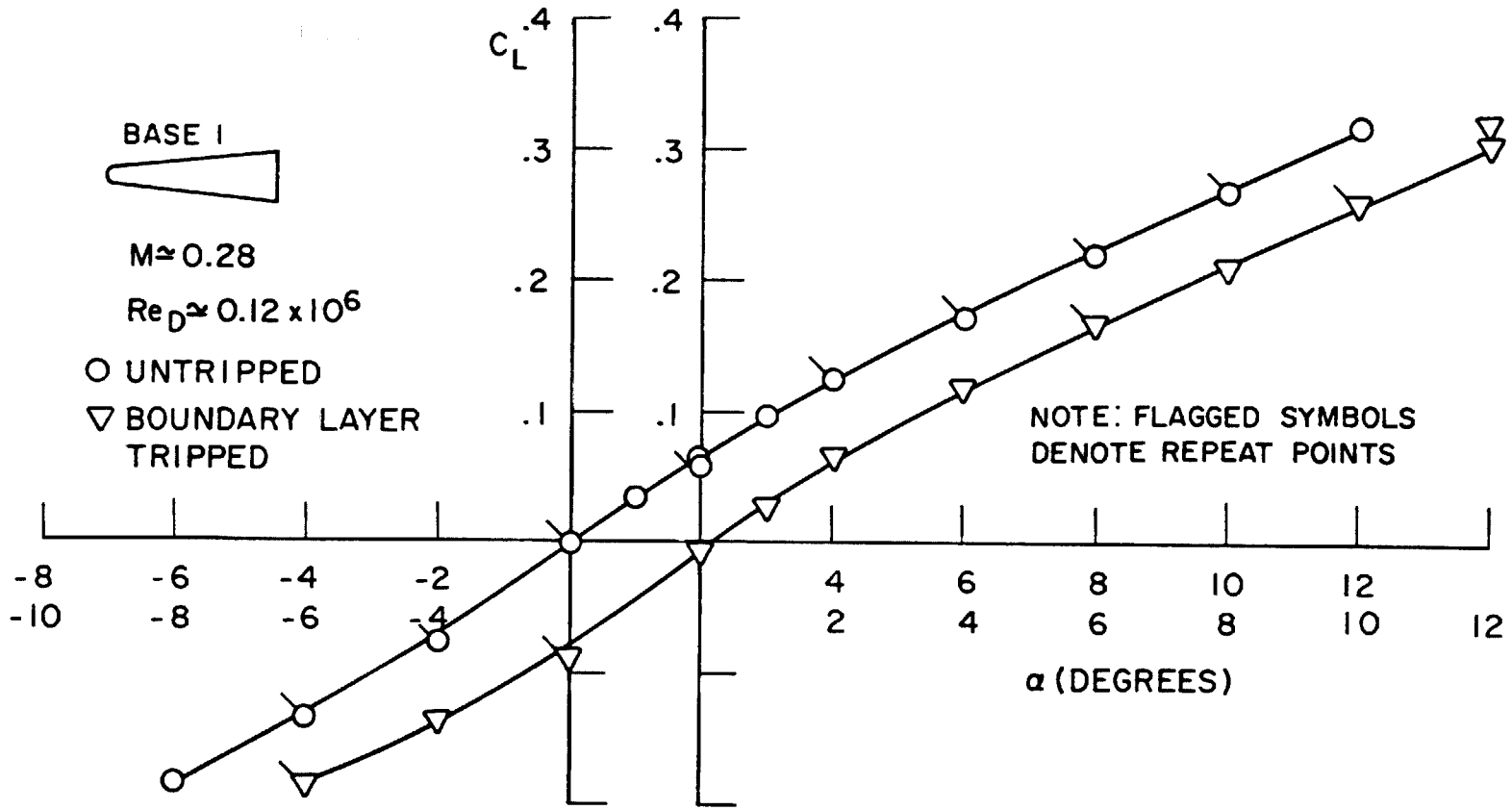

Figure 6. Subsonic Lift Coefficient versus Angle of Attack (Base 1 Model)

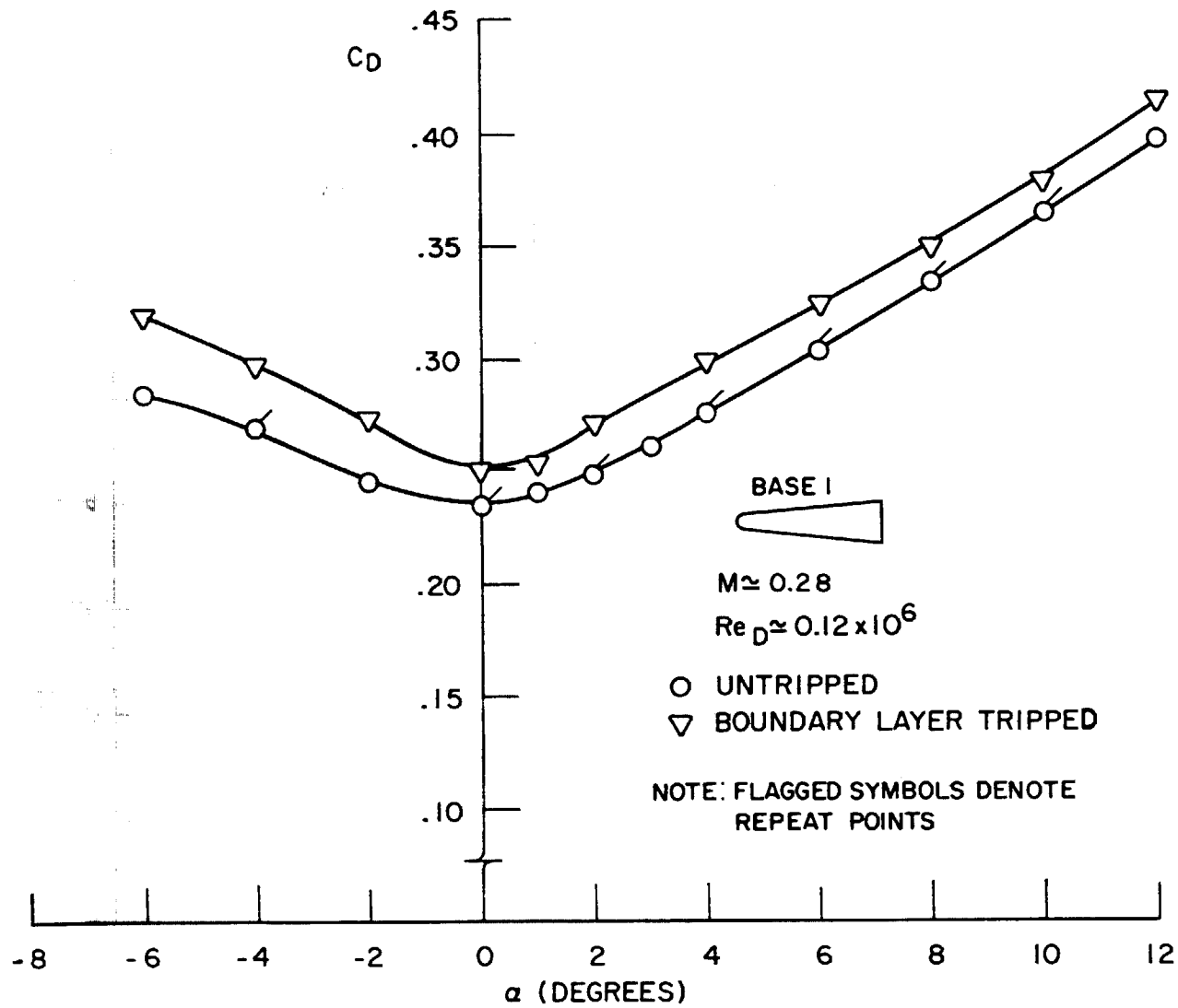

Figure 7. Subsonic Drag Coefficient versus Angle of Attack (Base 1 Model)

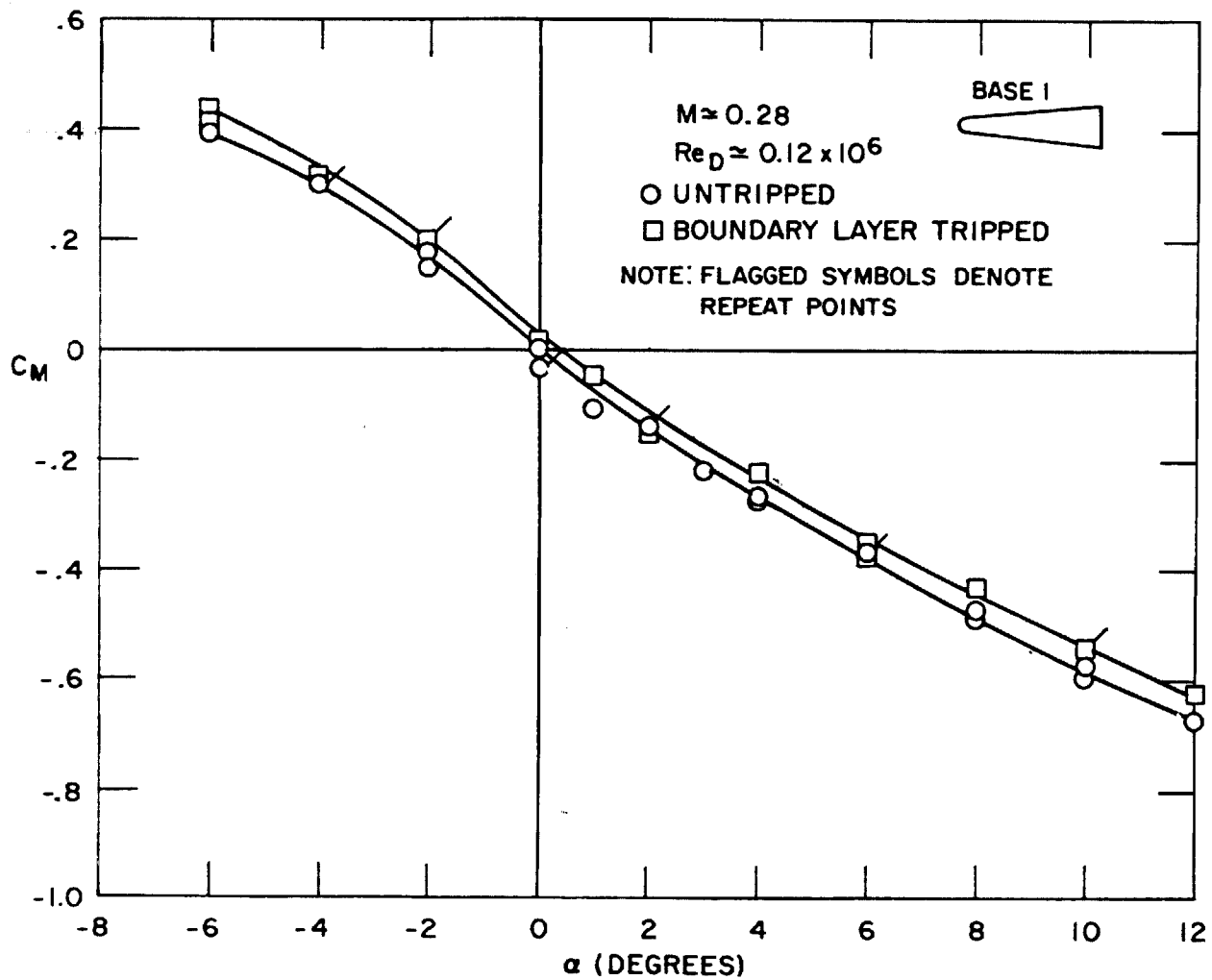

Figure 8. Subsonic Pitching Moment Coefficient versus Angle of Attack (Base 1 Model)

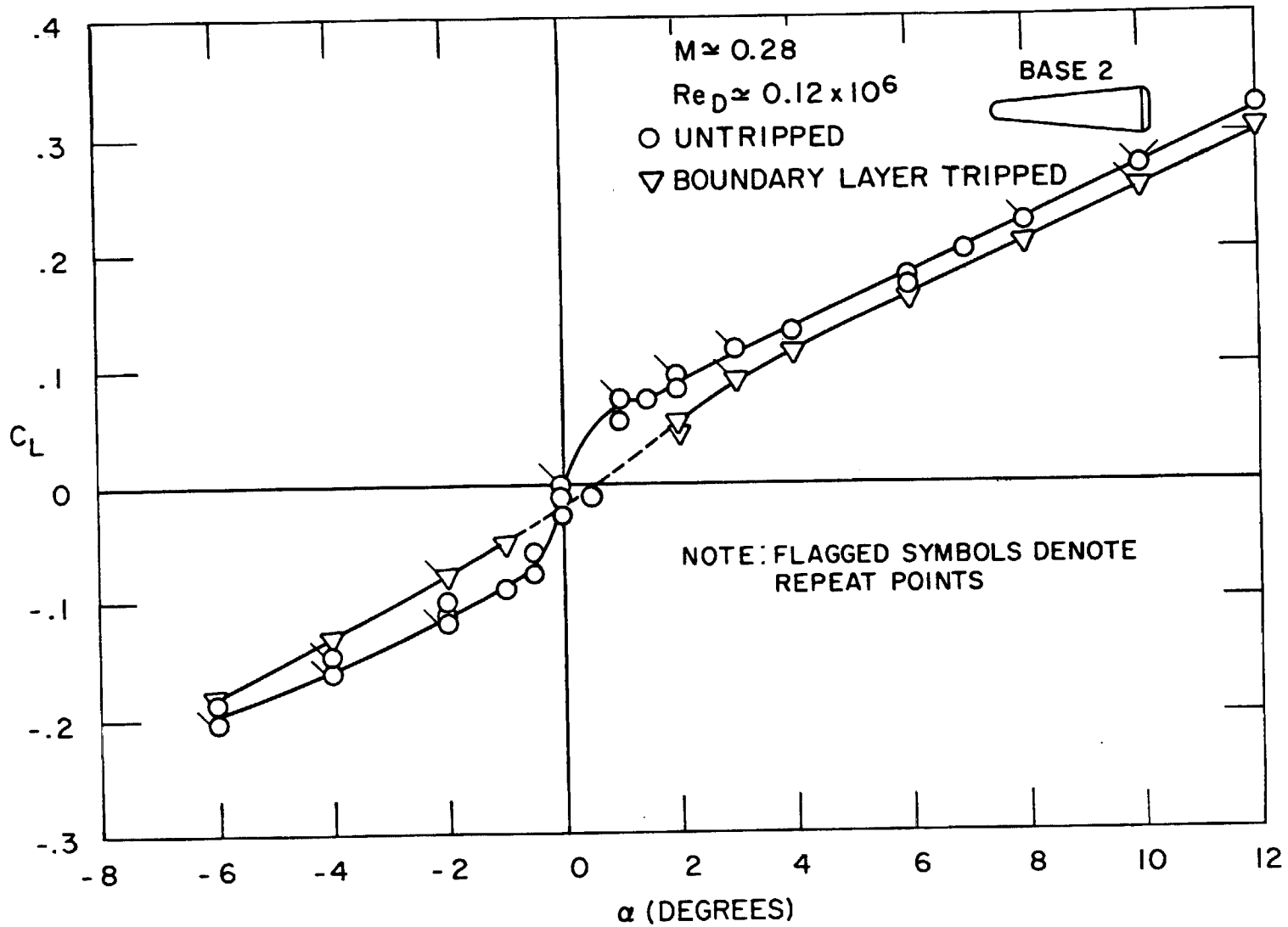

Figure 9. Subsonic Lift Coefficient versus Angle of Attack (Base 2 Model)

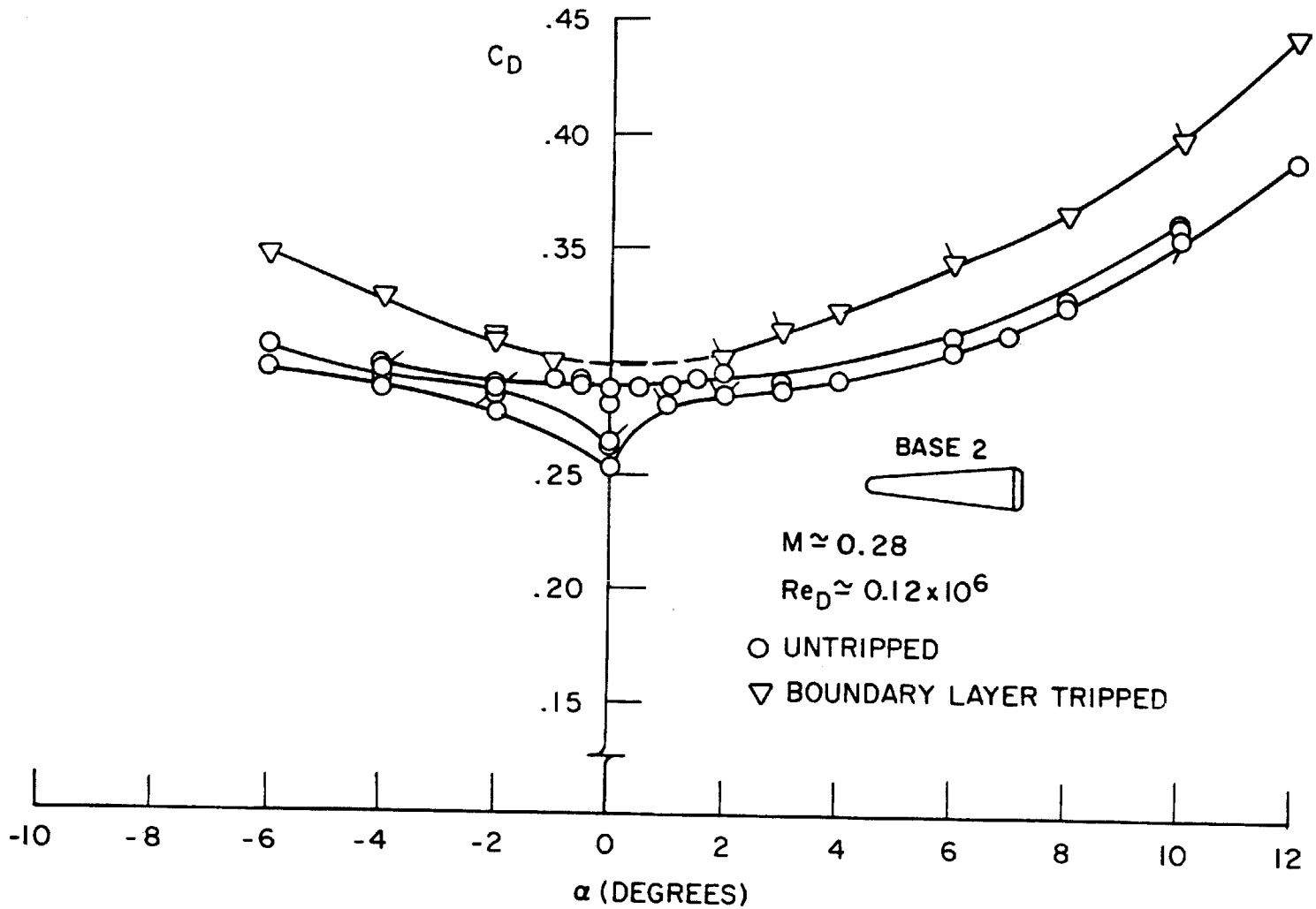

Figure 10. Subsonic Drag Coefficient versus Angle of Attack (Base 2 Model)

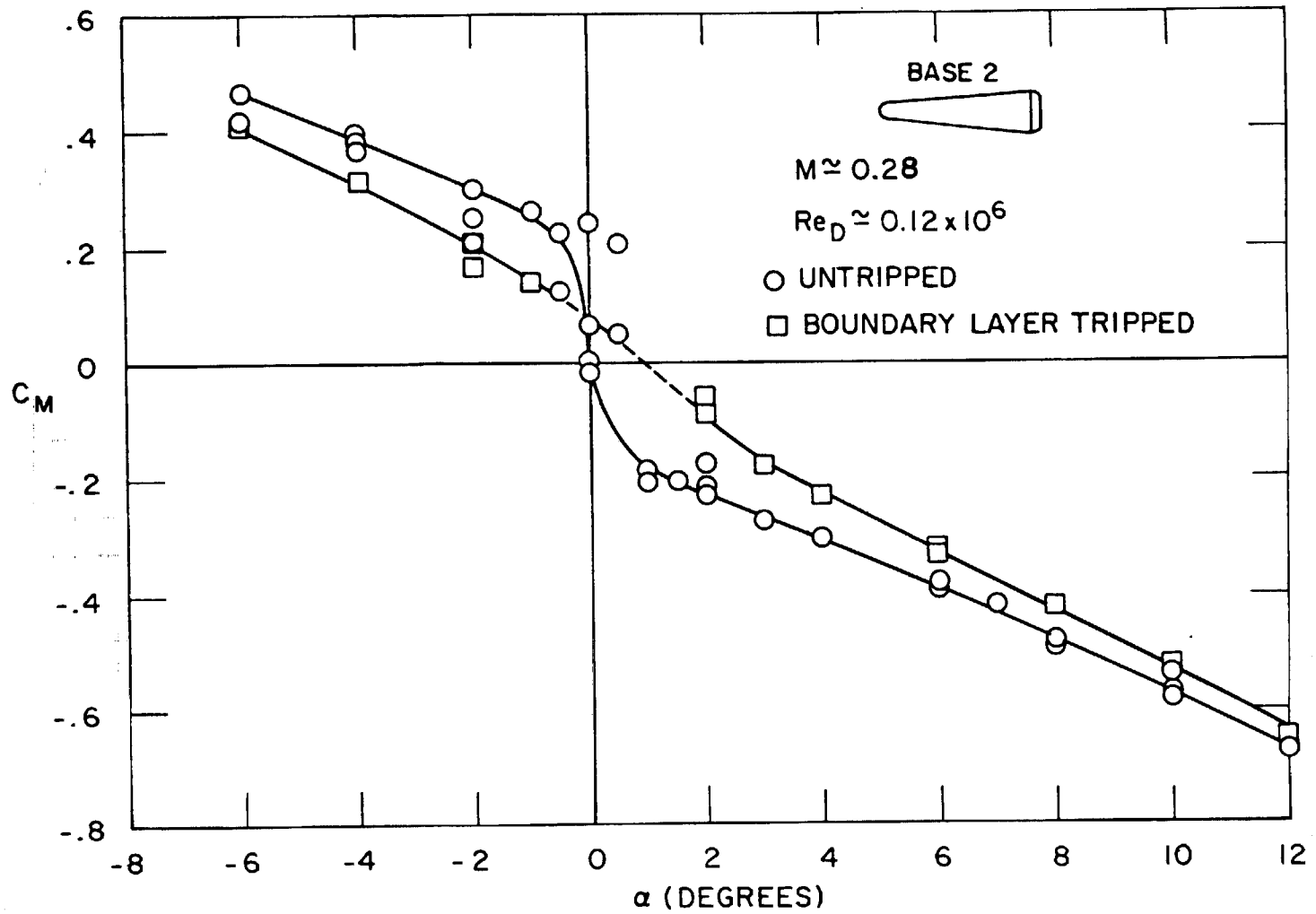

Figure 11. Subsonic Pitching Moment Coefficient versus Angle of Attack (Base 2 Model)

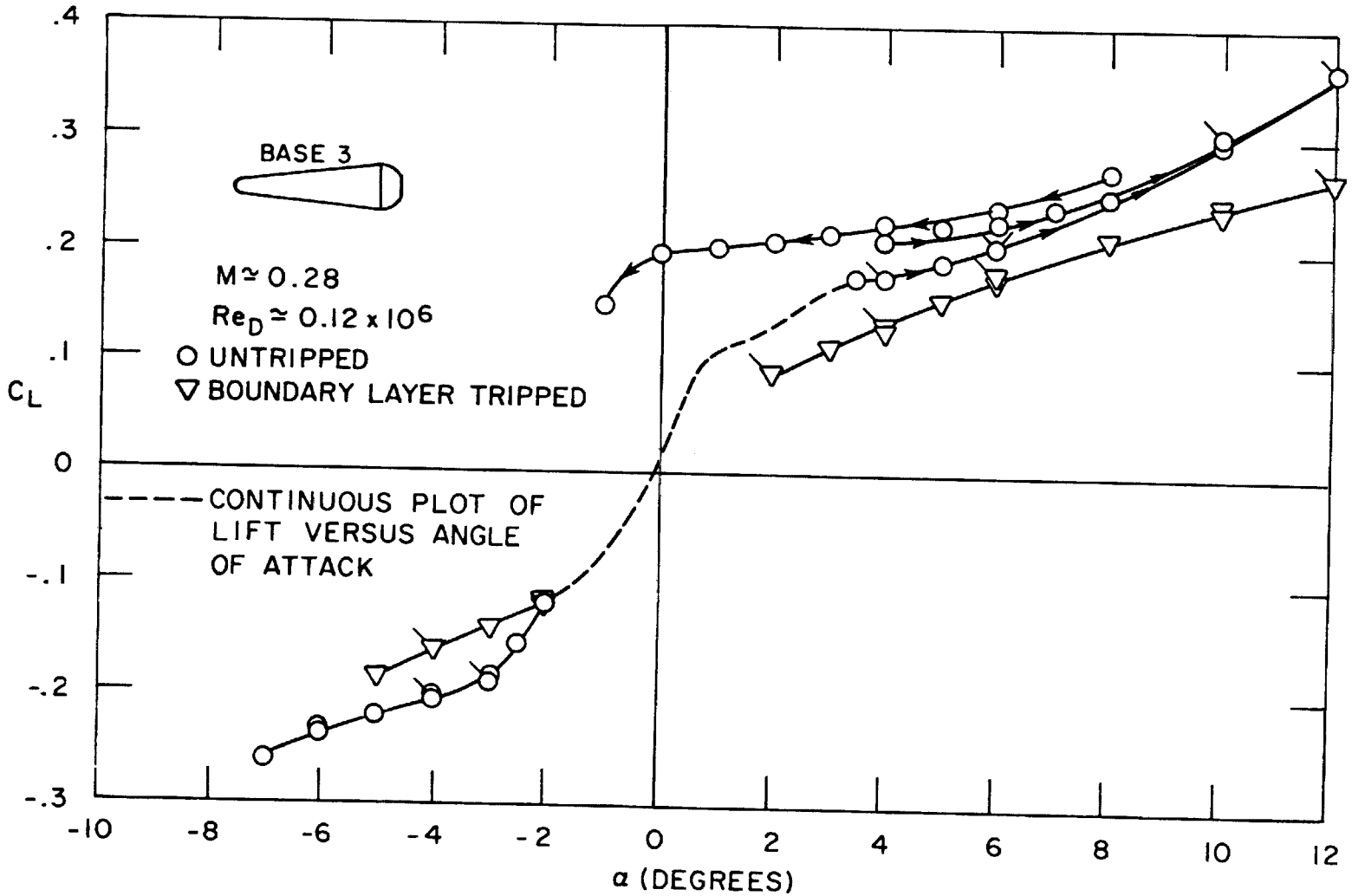

Figure 12. Subsonic Lift Coefficient versus Angle of Attack (Base 3 Model)

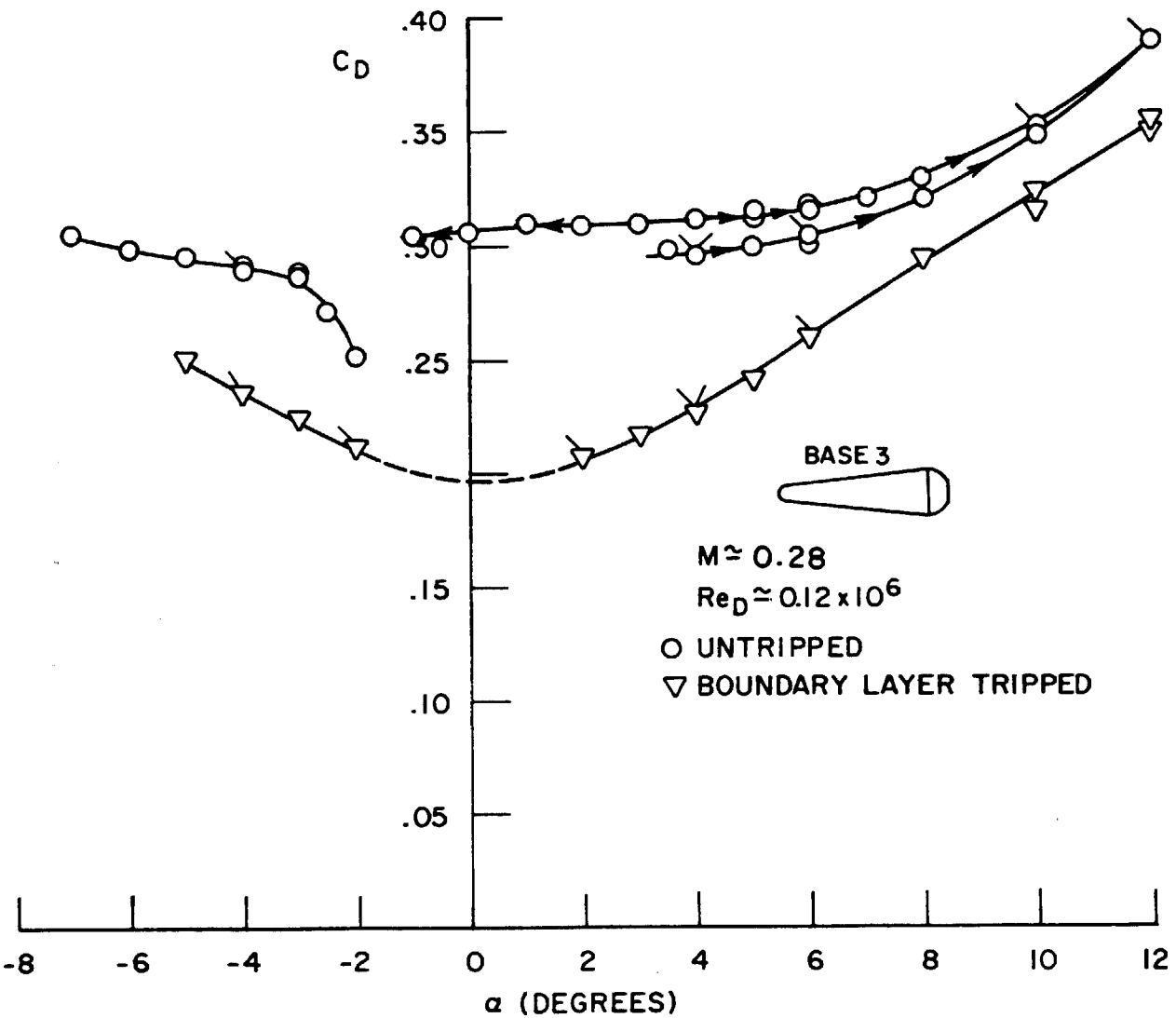

Figure 13. Subsonic Drag Coefficient versus Angle of Attack (Base 3 Model)

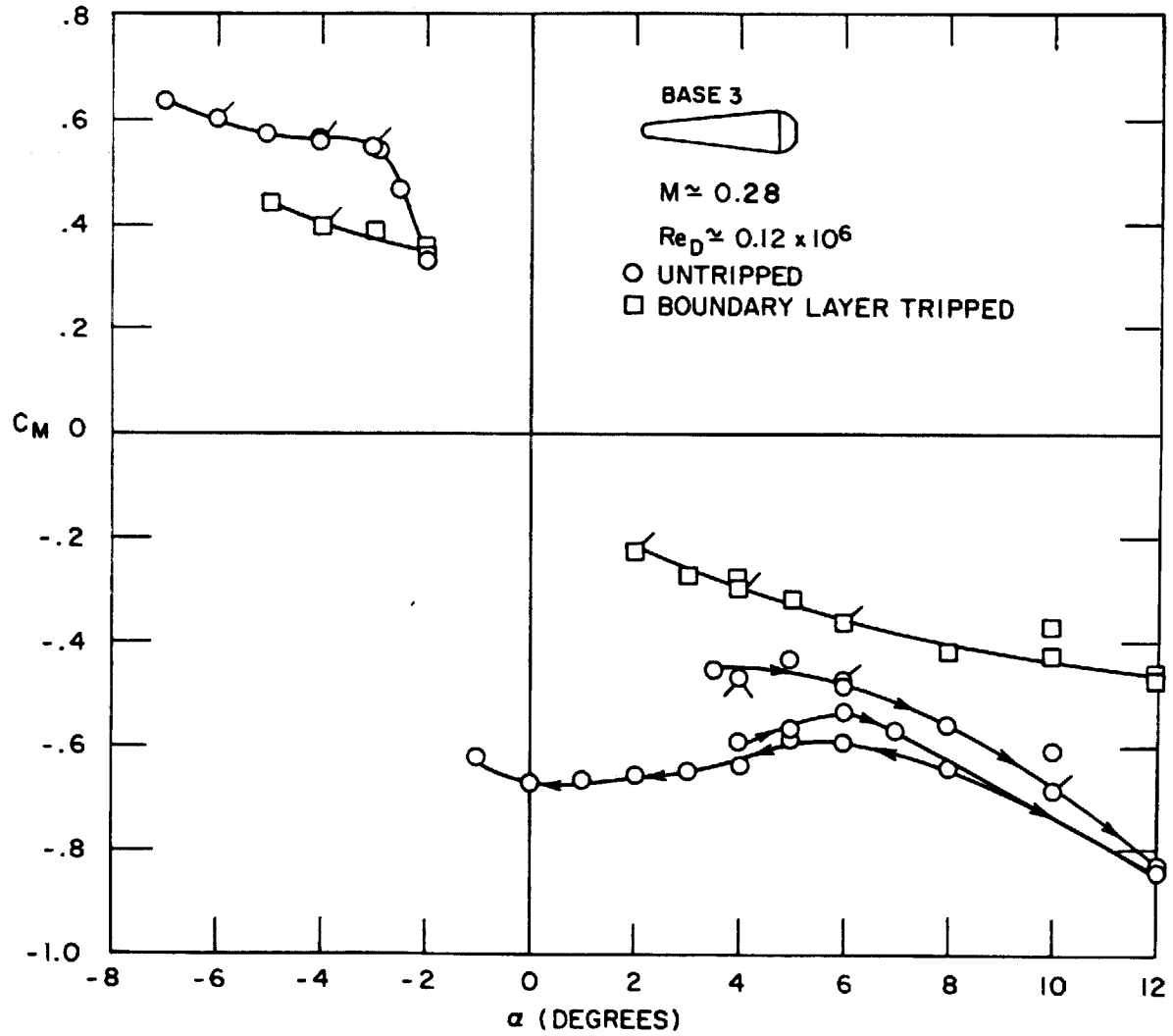

Figure 14. Subsonic Pitching Moment Coefficient versus Angle of Attack

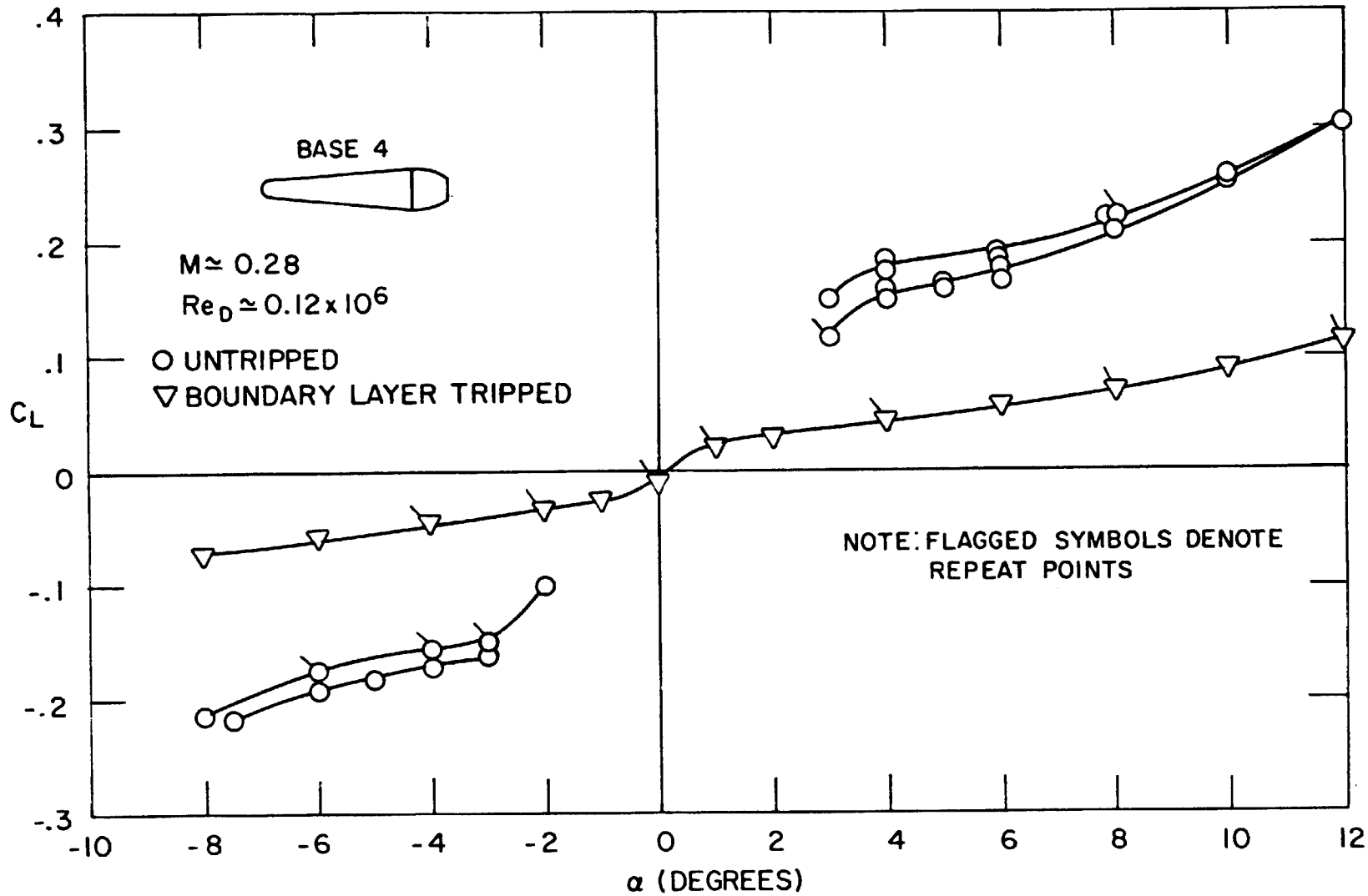

Figure 15. Subsonic Lift Coefficient versus Angle of Attack (Base 4 Model)

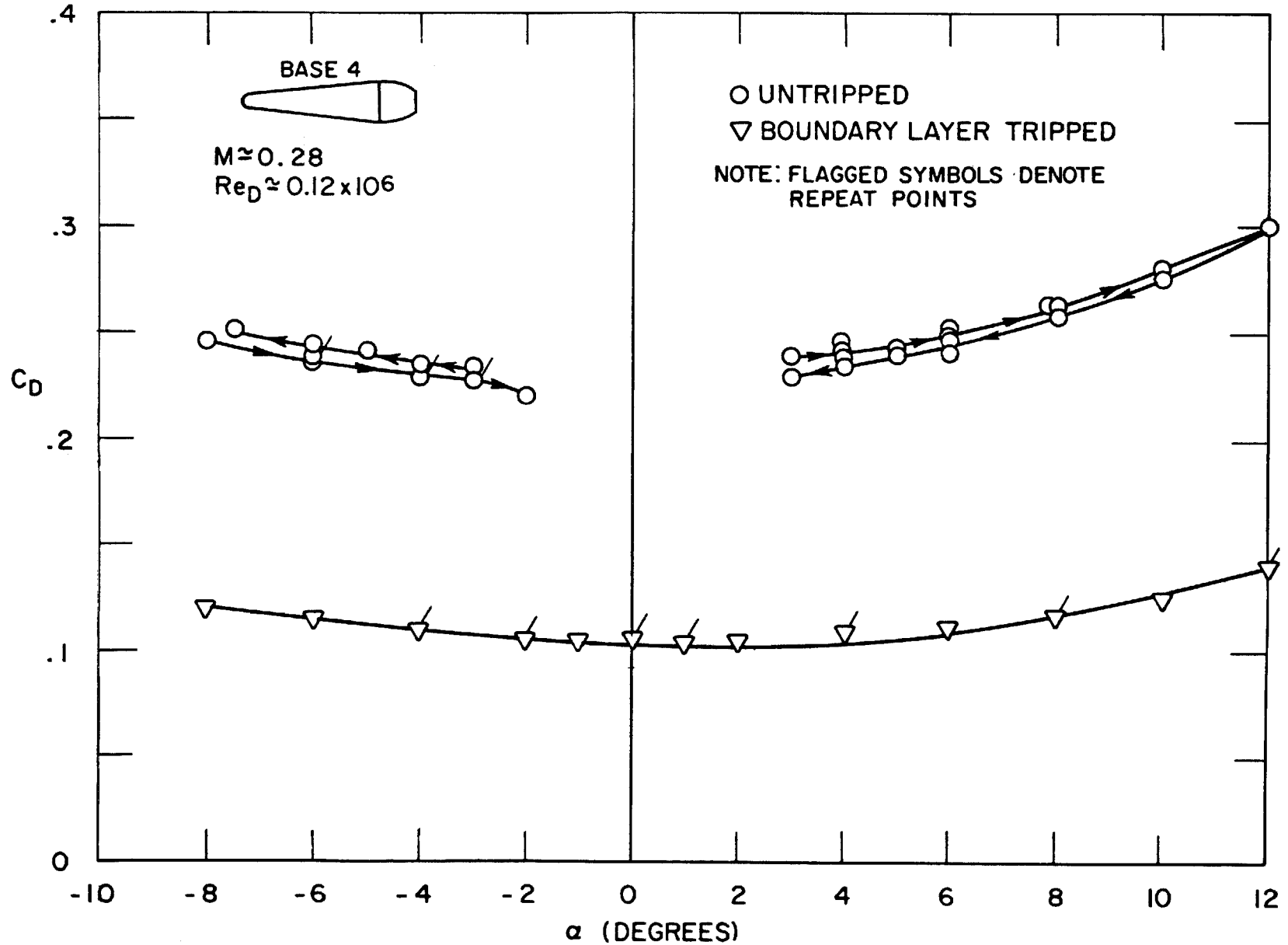

Figure 16. Subsonic Drag Coefficient versus Angle of Attack (Base 4 Model)

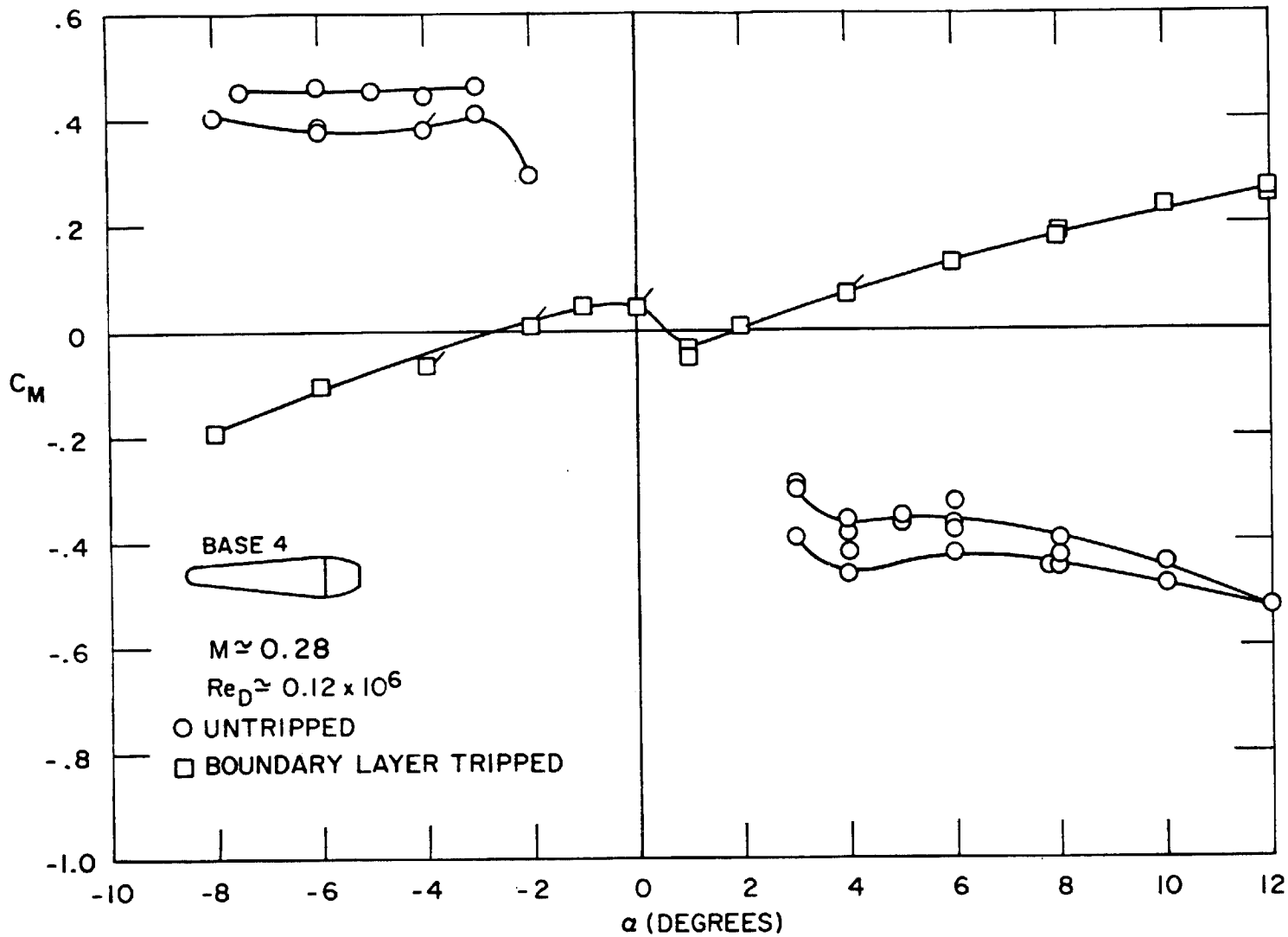

Figure 17. Subsonic Pitching Moment Coefficient versus Angle of Attack (Base 4 Model)

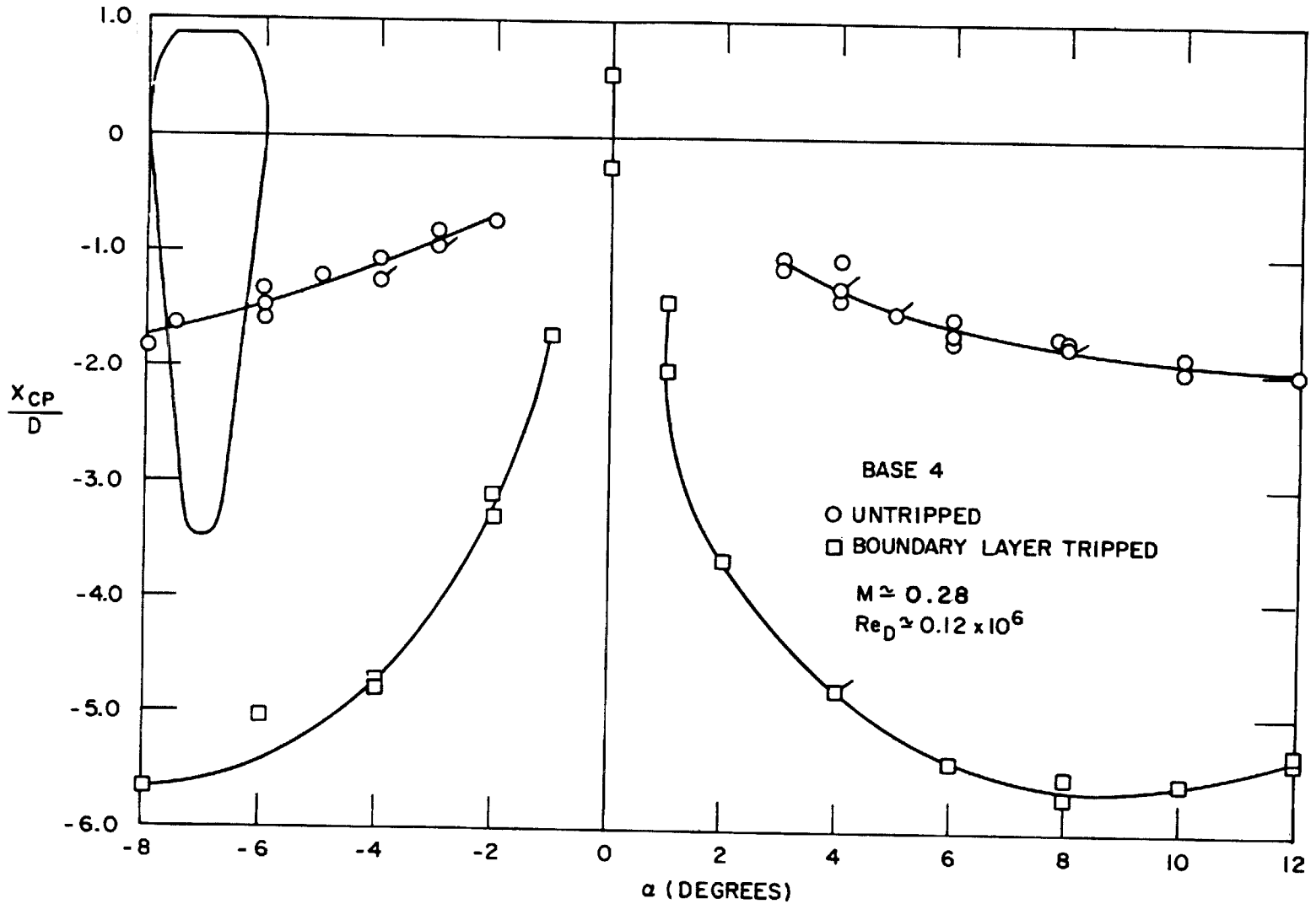

Figure 18. Subsonic Center of Pressure Location versus Angle of Attack (Base 4 Model)

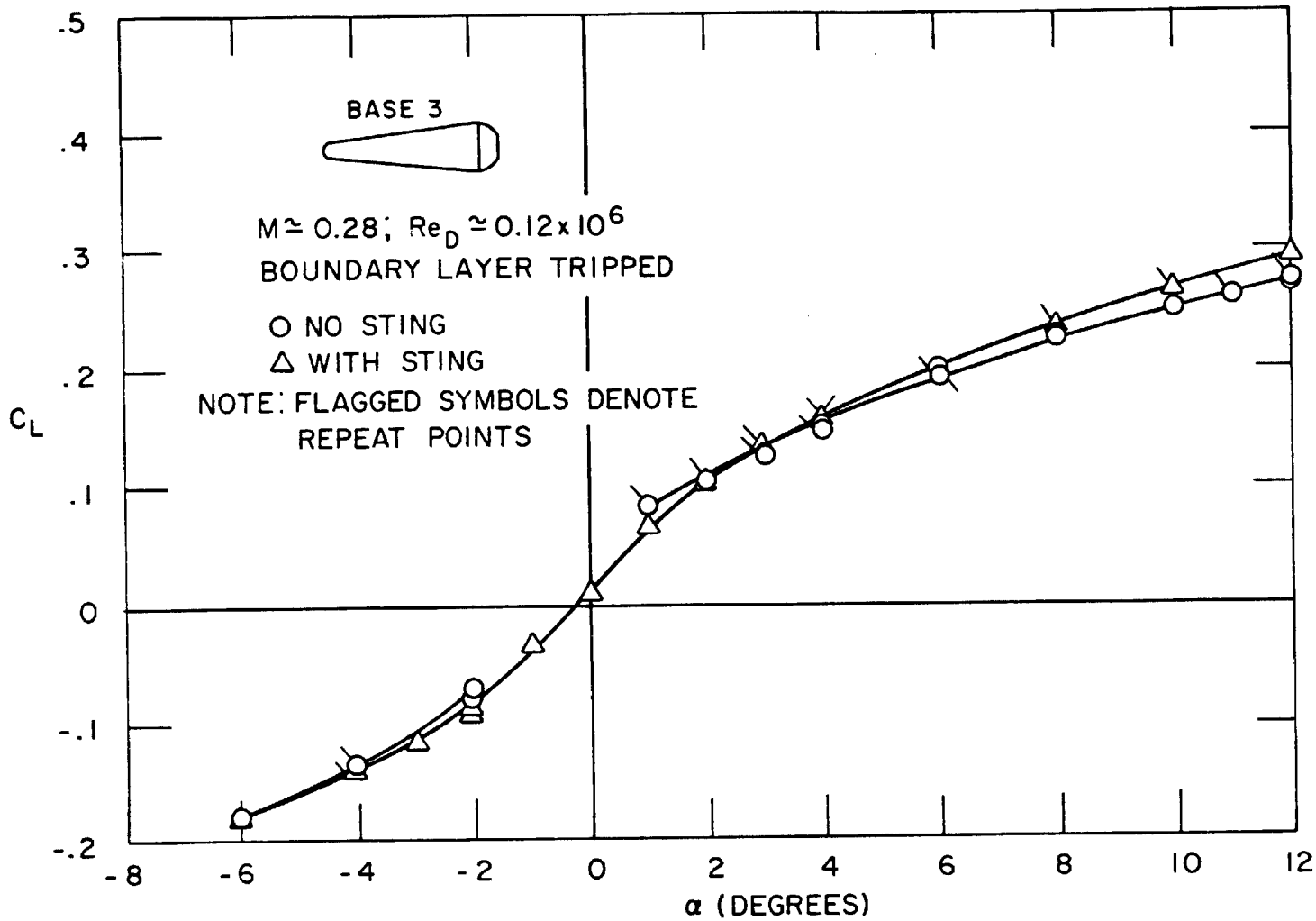

Figure 19. Effects of Sting Interference on the Lift Coefficient versus Angle of Attack (Base 3 Model)

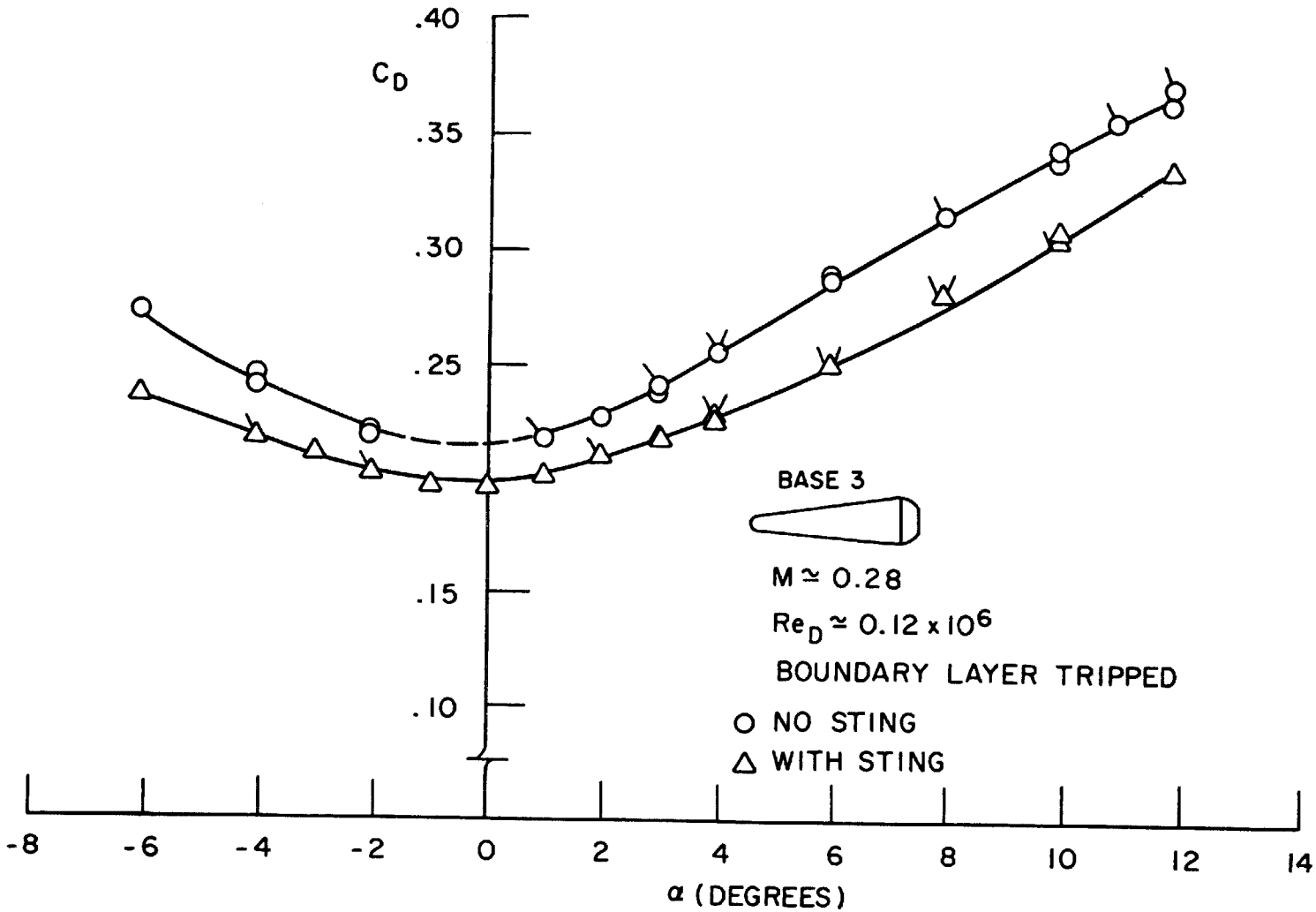

Figure 20. Effects of Sting Interference on the Drag Coefficient versus Angle of Attack (Base 3 Model)

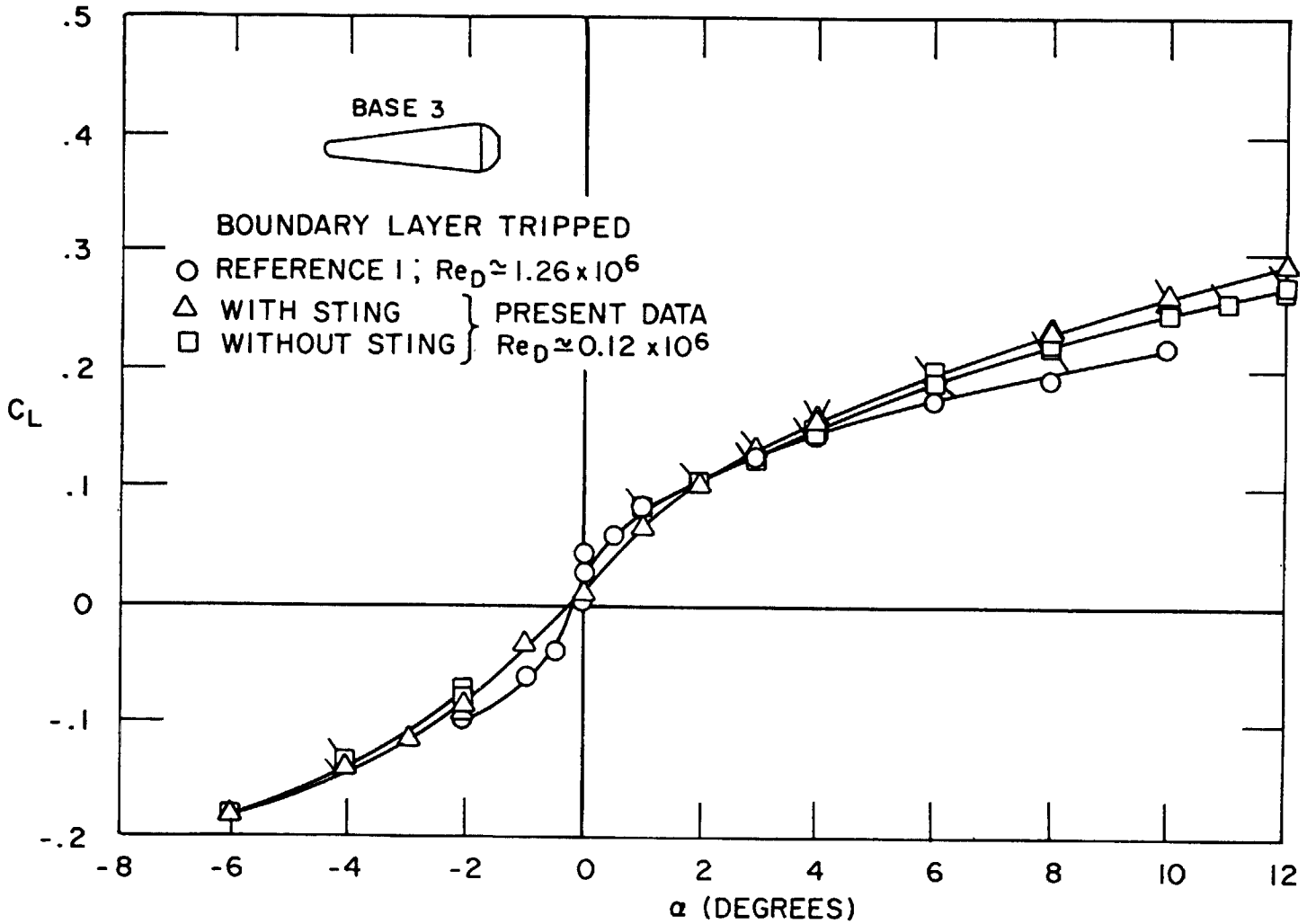

Figure 21. Subsonic Lift Coefficient versus Angle of Attack (Base 3 Model)